5 Genetic screen on homozygous gene traps

5.1 Introduction

During *in vitro* differentiation, ES cells can form cystic embryo-like aggregates, embryoid bodies (EB), that contain cells of endodermal, ectodermal and mesodermal lineages, which can further differentiate into more specialized cell types. The morphological changes of embryoid bodies are accompanied, at the molecular level, by the changes in the expression of a set of lineage-specific and tissue-specific markers. By comparing the dynamic changes in the expression of these markers *in vivo* and *in vitro*, different stages of EB differentiation *in vitro* can be linked to different stages of embryogenesis *in vivo* (Leahy, Xiong et al. 1999). These properties allow us to use ES cell *in vitro* differentiation as an *in vitro* model to study early embryogenesis and this facilitates genetic approaches.

5.1.1 *In vitro* differentiation protocols

There are three main protocols for ES cell *in vitro* differentiation: the hanging drop method (Wobus, Wallukat et al. 1991); the mass culture method (Doetschman, Eistetter et al. 1985); and the methylcellulose method (Wiles and Keller 1991). All three of these have been widely used for making embryoid bodies (EB) for different purposes.

The advantage of the hanging drop method is that the starting number of ES cells in an embryoid body is defined, so the size and the differentiation pattern of the EBs generated by this method is more consistent than with the other two methods. This characteristic is particularly important for developmental studies, which require the comparisons between EBs under different culture conditions and/or with different mutations (Wobus, Guan et al. 2002). However, this method is also more complicated than the other two methods.

On the other hand, the mass culture method is useful for differentiating a large number of ES cells. By plating undifferentiated ES cells onto bacteriological Petri dishes, the cells automatically form cell aggregates, and the aggregates can differentiate into a variety of different cell types. However, the size and the differentiation pattern can vary significantly between plates or between

experiments, even when the same ES cell line is used. The methylcellulose method is used specifically for the differentiation of haematopoietic lineages, and is not suitable for other purposes.

In this project, it was necessary to compare the *in vitro* differentiation potential of a number of homozygous mutant ES cell clones. Therefore the hanging drop method was the most appropriate *in vitro* differentiation protocol to use.

5.1.2 Parameters influencing *in vitro* differentiation of ES cells

The developmental potency of ES cells in culture is dependent on a number of intrinsic and extrinsic parameters. These include the number of ES cells used to make the EBs; the composition of the differentiation medium; cellular growth factors and differentiation inducers added to the culture medium; the ES cell lines; as well as the genetic changes in the ES cell genome.

Compared to *in vivo* differentiation in the mouse, the parameters for *in vitro* differentiation are more controllable. Whichever differentiation protocol is chosen, extrinsic parameters can be effectively controlled by using defined medium and culture conditions. Variations caused by intrinsic parameters can be eliminated by choosing an appropriate control ES cell line. Thus loss-of-function or gain-of-function studies using *in vitro* differentiation can be an ideal alternative to study the phenotypes of mutations on embryogenesis and early development (Wobus, Guan et al. 2002).

5.1.3 Recessive genetic screens using ES cell *in vitro* differentiation

Genetic analysis of recessive mutations in ES cells is informative on possible functions *in vivo*, especially for mutations that result in embryonic lethality. A recessive genetic screen using ES cell *in vitro* differentiation can be used to identify important genes in the differentiation process.

The bottleneck of recessive genetic screens in ES cells is the difficulty of obtaining enough homozygous mutant ES cells. If a genetic screen is performed to identify genes involved in ES cell *in vitro* differentiation, pure homozygous mutant ES cell clones need to be differentiated individually to

check for their differentiation potential. Existing methods to generate homozygous mutations in ES cells are not ideal for this purpose. In the previous chapters, I have demonstrated that a strategy combining regional trapping and inducible mitotic recombination can be used to generate homozygous mutations in a genomic region of interest. By Splinkerette PCR and 5' RACE, proviral/host flanking genomic sequences and/or cDNA sequence were isolated to identify the proviral insertion sites and inversion breakpoints of these mutant clones.

A total of 30 different gene-trap loci on chromosome 11 that are homozygously mutated were isolated. These homozygous gene-trap clones can be used to perform a small-scale genetic screen to identify the mutations that will disrupt the normal ES *in vitro* differentiation process. Each gene-trap clone has been differentiated individually, and a set of important lineage-specific and tissue-specific markers have been checked to determine the differentiation potential of each of the homozygous mutant ES cell lines. Mutant cell lines that show an abnormal differentiation pattern have been confirmed using independent methods.

5.2 Results

5.2.1 Primary screen

For each of the 33 mapped gene-trap loci, at least one subclone was chosen for the primary *in vitro* differentiation screen. Embryoid bodies were made and cultured as described before (Wobus, Guan et al. 2002). In brief, undifferentiated ES cells were maintained on feeder layers until they were used for *in vitro* differentiation. To setup the assay, ES cells were trypsinized and diluted to a final concentration of approximately 600 cells in 20 μl Differentiation Medium (see material and methods). 20 μl drops of the ES cell suspension were laid onto the bottom of 100-mm bacteriological Petri dishes. The Petri dishes were inverted and the ES cell aggregates were cultured in the resulting hanging drops for two days. After this, the Petri dishes were turned the right way up and Differentiation Medium was added into each dish to rinse the aggregates. The aggregates were cultured in suspension for

another three days. The sample was harvested at Day 5. At the same time, the EBs on the remaining dishes were plated out onto gelatinized 90-mm tissue culture plates. The plated EBs were subsequently cultured in Differentiation Medium supplemented with 10^{-8} M retinoic acid (RA) and the medium was changed every two days. Subsequent samples were taken at Day 8 and Day 11.

When all the samples were taken, RNA was extracted from each sample and quantified. 5 μg total RNA was used for first strand cDNA synthesis. The resulting cDNA was used as a template for RT-PCR. In the primary of screen, 16 pairs of primers were used (*Afp*, *β-Actin*, *Brachyury*, *Bmp4*, *Ctla4*, *Cx40*, *Cx45*, *Fyn*, *Gata4*, *Goosecoid*, *Hnf4*, *Nodal*, *Oct3/4*, *Pecam*, *Tie2* and *vHNF1*). All the homozygous mutant cell lines that showed abnormal expression (significant up-regulation or down-regulation compared to the WW93A12 control line) for one or more markers in the primary screen were selected for the second round screen (Fig. 5-1 and Fig. 5-2).

All the mitotic recombination clones (WW103) used in the screen carry two homologs of chromosome 11 from the same parent, either bi-paternal or bi-maternal. It is possible that because of the imprinting, the *in vitro* differentiation pattern of ES cells carrying bi-paternal or bi-maternal homologs of chromosome 11 will be different from that of the wild-type ES cells that have one paternal and one maternal homologs of chromosome 11. Also, the *in vitro* differentiation potential of ES cells homozygous for the targeted E_2DH allele has not been assessed. So an ideal control cell line for this experiment will carry two homologs of chromosome 11 from the same parent as the WW103 clones, and this control cell line is also homozygous for the targeted E_2DH allele.

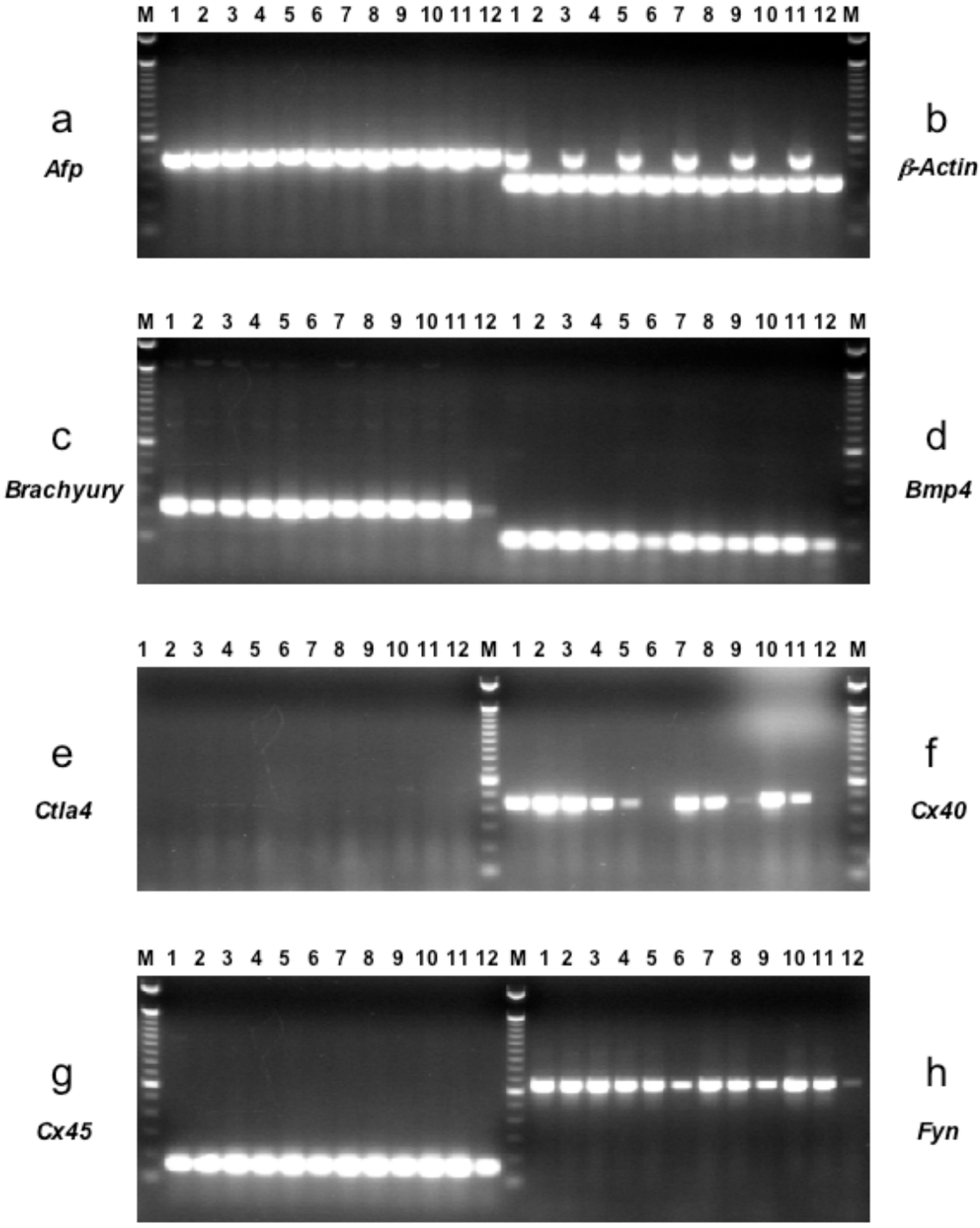
M 1 2 3 4 5 6 7 8 9 10 11 12 1 2 3 4 5 6 7 8 9 10 11 12 M
a
Afp
b
β-Actin
M 1 2 3 4 5 6 7 8 9 10 11 12 1 2 3 4 5 6 7 8 9 10 11 12 M
c
Brachyury
d
Bmp4
1 2 3 4 5 6 7 8 9 10 11 12 M 1 2 3 4 5 6 7 8 9 10 11 12 M
e
Ctla4
f
Cx40
M 1 2 3 4 5 6 7 8 9 10 11 12 M 1 2 3 4 5 6 7 8 9 10 11 12
g
Cx45
h
Fyn

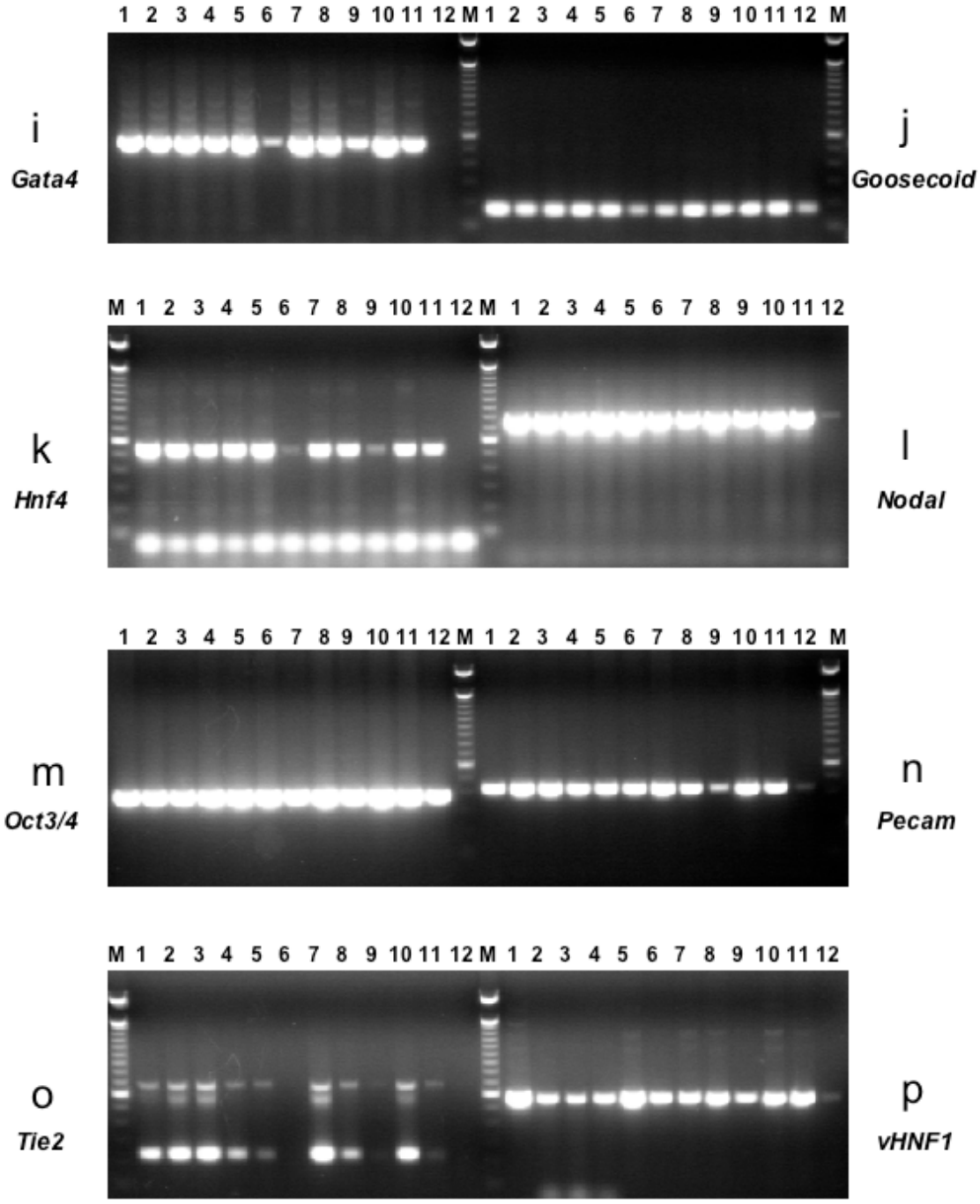
1 2 3 4 5 6 7 8 9 10 11 12 M 1 2 3 4 5 6 7 8 9 10 11 12 M
i
Gata4
j
Goosecoid
M 1 2 3 4 5 6 7 8 9 10 11 12 M 1 2 3 4 5 6 7 8 9 10 11 12
k
Hnf4
l
Nodal
1 2 3 4 5 6 7 8 9 10 11 12 M 1 2 3 4 5 6 7 8 9 10 11 12 M
m
Oct3/4
n
Pecam
M 1 2 3 4 5 6 7 8 9 10 11 12 M 1 2 3 4 5 6 7 8 9 10 11 12
o
Tie2
p
vHNF1

Fig. 5-1 RT-PCR results of Day 5 embryoid bodies. a. *Afp*. **b.** *β-Actin*. Note that line 1, 3, 5, 7, 9 and 11 were mistakenly mixed with PCR products from **a**. *β-Actin* was used as a loading control. **c.** *Brachyury*. **d.** *Bmp4*. **e.** *Ctla4*. **f.** *Cx40*. **g.** *Cx45*. **h.** *Fyn*. **i.** *Gata4*. **j.** *Goosecoid*. **k.** *Hnf4*. **l.** *Nodal*. **m.** *Oct3/4*. **n.** *Pecam*. **o.** *Tie2*. **p.** *vHNF1*. Lane 1, WW103-16B3; 2, WW103-16D2; 3, WW103-17F2; 4, WW103-17G6; 5, WW103-18E8; 6, WW103-18F11; 7, WW103-18G10; 8, WW103-19A1; 9, WW103-19A2; 10, WW103-19A6; 11, WW103-19A8; 12, WW103-19D3; M, 100 bp ladder (Invitrogen)

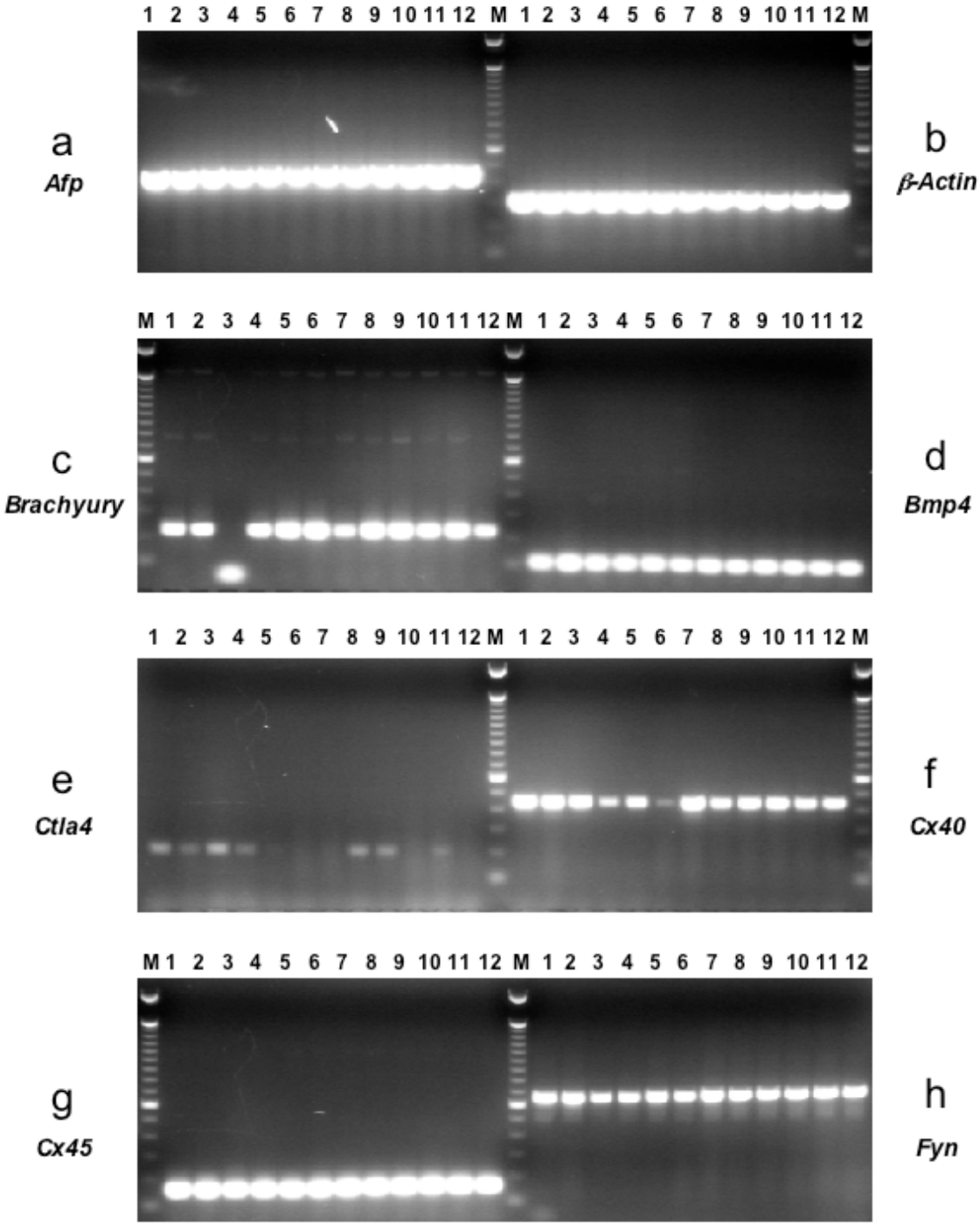
1 2 3 4 5 6 7 8 9 10 11 12 M 1 2 3 4 5 6 7 8 9 10 11 12 M
a
Afp
b
β-Actin
M 1 2 3 4 5 6 7 8 9 10 11 12 M 1 2 3 4 5 6 7 8 9 10 11 12
c
Brachyury
d
Bmp4
1 2 3 4 5 6 7 8 9 10 11 12 M 1 2 3 4 5 6 7 8 9 10 11 12 M
e
Ctla4
f
Cx40
M 1 2 3 4 5 6 7 8 9 10 11 12 M 1 2 3 4 5 6 7 8 9 10 11 12
g
Cx45
h
Fyn

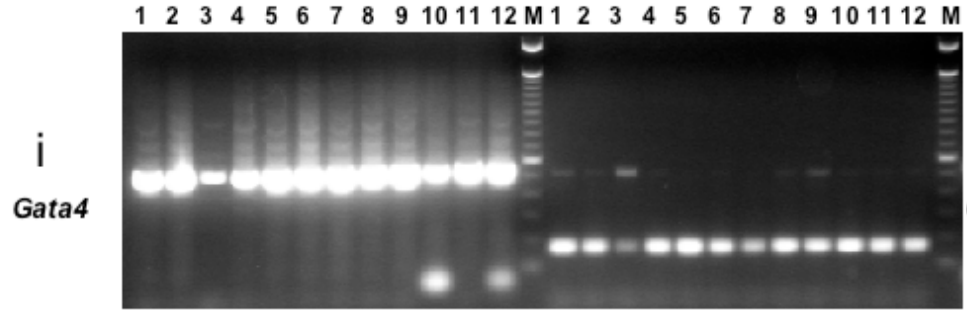

i
Gata4

j
Goosecoid

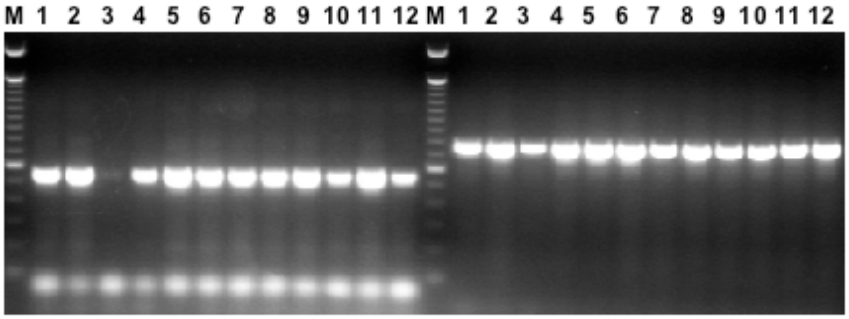

k
Hnf4

l
Nodal

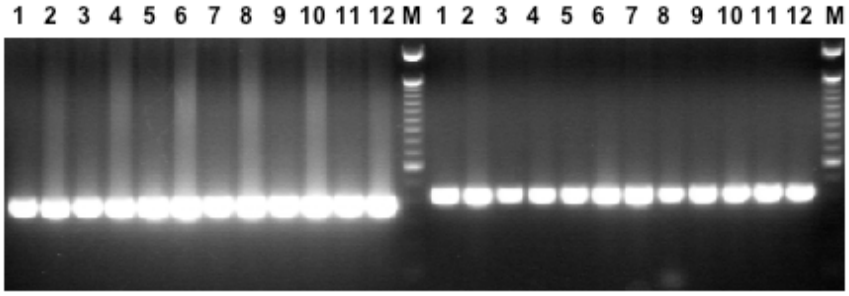

m
Oct3/4

n
Pecam

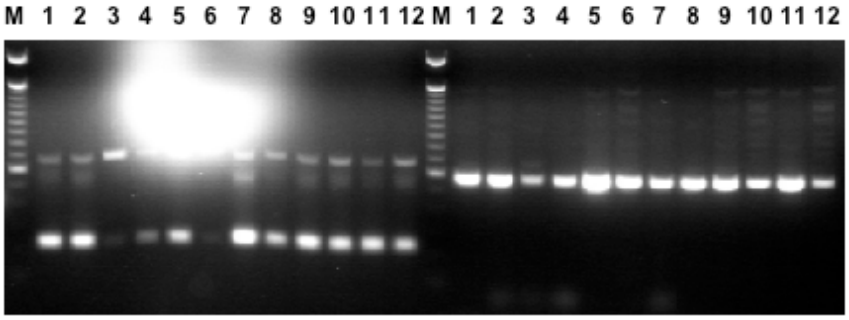

o
Tie2

p
vHNF1

Fig. 5-2 RT-PCR result of Day 8 embryoid bodies. a. *Afp*. **b.** *β-Actin*. **c.** *Brachyury*. **d.** *Bmp4*. **e.** *Ctla4*. **f.** *Cx40*. **g.** *Cx45*. **h.** *Fyn*. **i.** *Gata4*. **j.** *Goosecoid*. **k.** *Hnf4*. **l.** *Nodal*. **m.** *Oct3/4*. **n.** *Pecam*. **o.** *Tie2*. **p.** *vHNF1*. Lane 1, WW103-16B3; 2, WW103-16D2; 3, WW103-17F2; 4, WW103-17G6; 5, WW103-18E8; 6, WW103-18F11; 7, WW103-18G10; 8, WW103-19A1; 9, WW103-19A2; 10, WW103-19A6; 11, WW103-19A8; 12, WW103-19D3; M, 100 bp ladder (Invitrogen)

To generate this control ES cell line, a Cre expression plasmid was electroporated into the WW69-D6 cell line and mitotic recombination clones were selected in M15 supplemented with HAT. The clones with the desired phenotype were identified both by sib-selection and by Southern analysis using an *E_2DH* 3' probe. The G2-X recombinants are resistant to HAT and blasticidin, but sensitive to G418 and puromycin. Southern analysis of *Nde*I digested genomic DNA will generate a 9.6 kb targeted fragment instead of the 13.1 kb wild-type fragment. One clone with the desired genotype, WW93-A12 and its subclones were used as controls in the ES cell *in vitro* differentiation screen.

5.2.2 Secondary screen

Mutant cell lines that showed an abnormal expression pattern for the markers checked in the primary screen were subcloned and single colonies were picked to avoid cross-contamination by ES cells that did not have the correct genotype. The control cell line, WW93-A12 was also subcloned. Southern analysis was performed on all the subclones to confirm their identities (Fig. 5-3).

The *in vitro* differentiation protocol for the second round screen is essentially the same as that of the first round. But more time points were taken and more molecular markers were checked using RT-PCR. The clones that still showed abnormal expression for the markers checked were characterized individually.

5.2.3 WW103-8E6 (*Pecam*)

One of the mitotic recombination clones, WW103-8E6, have overtly impaired *in vitro* differentiation potential. When the EBs were plated onto the gelatinized tissue culture plates, the EBs could not form cystic three-dimensional structures. When RT-PCR was performed using a series of molecular markers, the expression of some markers in the day 8 EBs was significantly down-regulated compared to the wild-type control, WW93-A12 (Fig. 5-4).

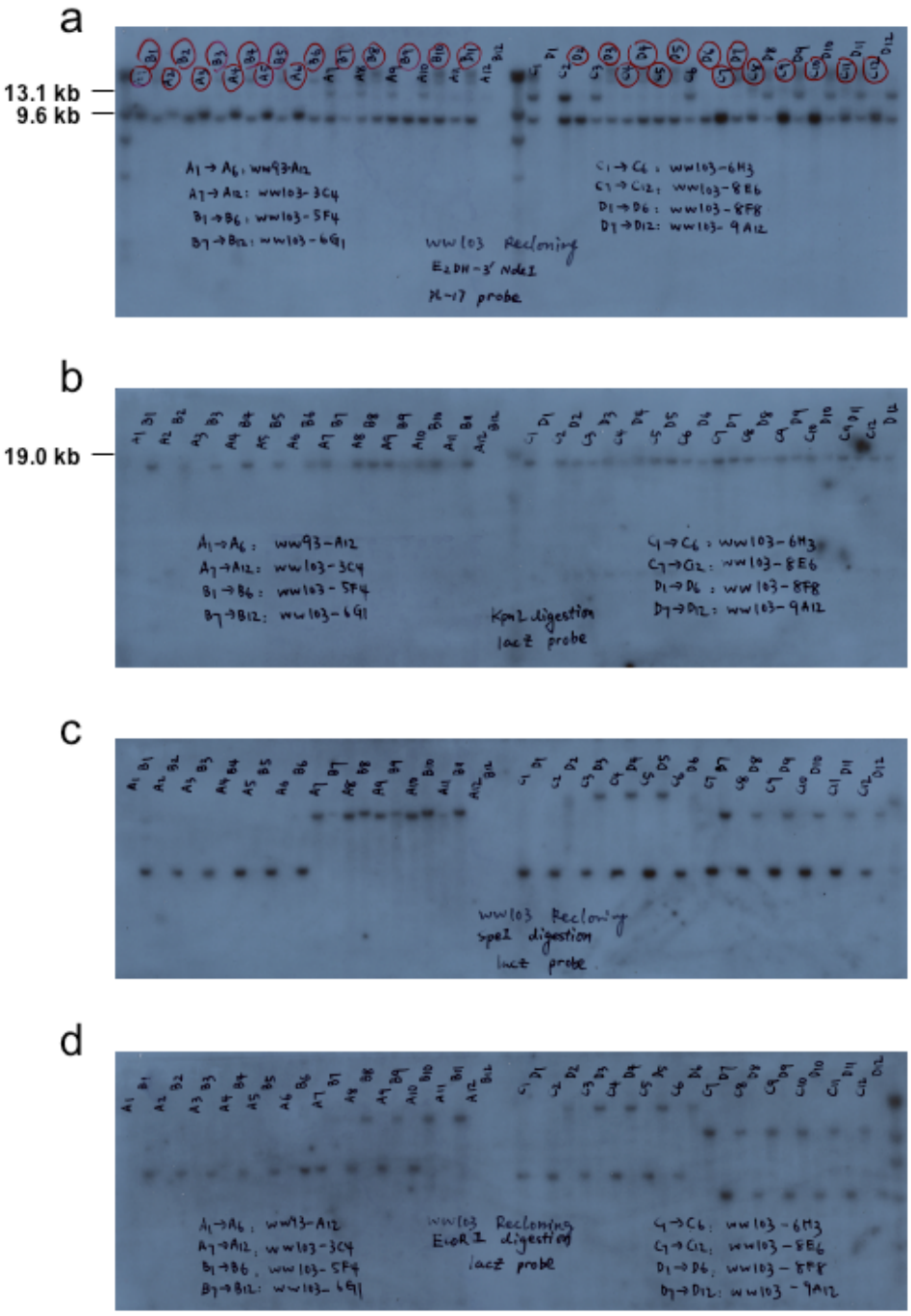
a
13.1 kb
9.6 kb
A1→A6: ww93-A12
A7→A12: ww103-3C4
B1→B6: ww103-5F4
B7→B12: ww103-6G1
ww103 Recloning
E2DH-3' NdeI
PL-17 probe
C1→C6: ww103-6H3
C7→C12: ww103-8E6
D1→D6: ww103-8F8
D7→D12: ww103-9A12
b
19.0 kb
A1→A6: ww93-A12
A7→A12: ww103-3C4
B1→B6: ww103-5F4
B7→B12: ww103-6G1
KpnI digestion
lacZ probe
C1→C6: ww103-6H3
C7→C12: ww103-8E6
D1→D6: ww103-8F8
D7→D12: ww103-9A12
c
ww103 Recloning
SpeI digestion
lacZ probe
d
A1→A6: ww93-A12
A7→A12: ww103-3C4
B1→B6: ww103-5F4
B7→B12: ww103-6G1
ww103 Recloning
EcoRI digestion
lacZ probe
C1→C6: ww103-6H3
C7→C12: ww103-8E6
D1→D6: ww103-8F8
D7→D12: ww103-9A12

Fig. 5-3 Southern analysis of subclones of homozygous mutant ES cell lines. a. Genomic DNA from the subclones was cut with *Nde*I and hybridized to an E_2DH 3' probe. The targeted restriction fragment is 9.6 kb and the wild type fragment is 13.1 kb. Note that some subclones of WW103-6H3 (c1, c2, c3 and c6) are heterozygous. **b.** Genomic DNA from the subclones was cut with *Kpn*I and hybridized to a *lacZ* probe. A 19.0 kb inversion restriction fragment was detected for all the subclones except those of the control cell line, WW93-A12. **c.** Genomic DNA from the subclones was cut with *Spe*I and hybridized to a *lacZ* probe. Proviral/host junction fragments of different sizes were detected for all the subclones except those of the control cell line, WW93-A12. **d.** Genomic DNA from the subclones was cut with *Eco*RI and hybridized to a *lacZ* probe. Proviral/host junction fragments of different sizes were detected for all the subclones except those of the control cell line, WW93-A12.

The *Spe*I/*Xba*I/*Nhe*I Splinkerette PCR product from this clone mapped the proviral insertion site to the first intron of *Pecam* (Platelet endothelial cell Adhesion Molecule Precursor, CD31) (Fig. 5-5a). The 5' RACE product matched an alternative spliced exon (Exon 1b) (Fig. 5-5b). In the Ensembl browser, there are at least three different spliced forms at the 5' end of this gene. *Pecam* transcripts can start from Exon 1a, Exon 1b or a site just 5' to Exon2 (Fig. 5-5c). The open reading frame (ORF) of *PECAM* starts from Exon 2. So the breakpoint in intron 1 created by the inversion would disrupt the transcripts starting from Exon1a and 1b, but it may not affect the transcripts starting from Exon 2. RT-PCR primers were used to determine the expression of different alternative spliced forms of *Pecam* in undifferentiated WW93-A12 and WW103-8E6 ES cells. This analysis revealed that none of the transcripts in undifferentiated ES cells started from Exon 1a (data not shown). In undifferentiated WW93-A12 ES cells, most *Pecam* transcripts start from Exon 1b. However, in undifferentiated WW103-8E6 ES cells, *Pecam* transcripts starting from Exon 2 and Exon 1b were both detected, implying that the inversion did not completely block the transcription across the breakpoint (Fig. 5-5d).

The *in vitro* differentiation of another *Pecam* gene-trap clone, WW103-4A6, showed that the differentiation of this clone was not impaired by the proviral insertion and the breakage caused by inversion. The *Sau*3A1 Splinkerette PCR product fro this clone has mapped the proviral insertion site to the third intron of *Pecam* (Fig. 5-6a and b). RT-PCR analysis of WW103-4A6 during the process of differentiation showed the expression of all the molecular markers during differentiation which was the same as the control cell line, WW93-A12 (data not shown). RT-PCR using a pair of primers specifically designed to amplify Exons 6, 7 and 8 of *Pecam* showed that the Pecam expression was completely blocked in WW103-4A6. On the other hand, WW103-8E6 and WW103-8G9, subclones in the same group as 8E6, showed normal *Pecam* expression (Fig. 5-6c).

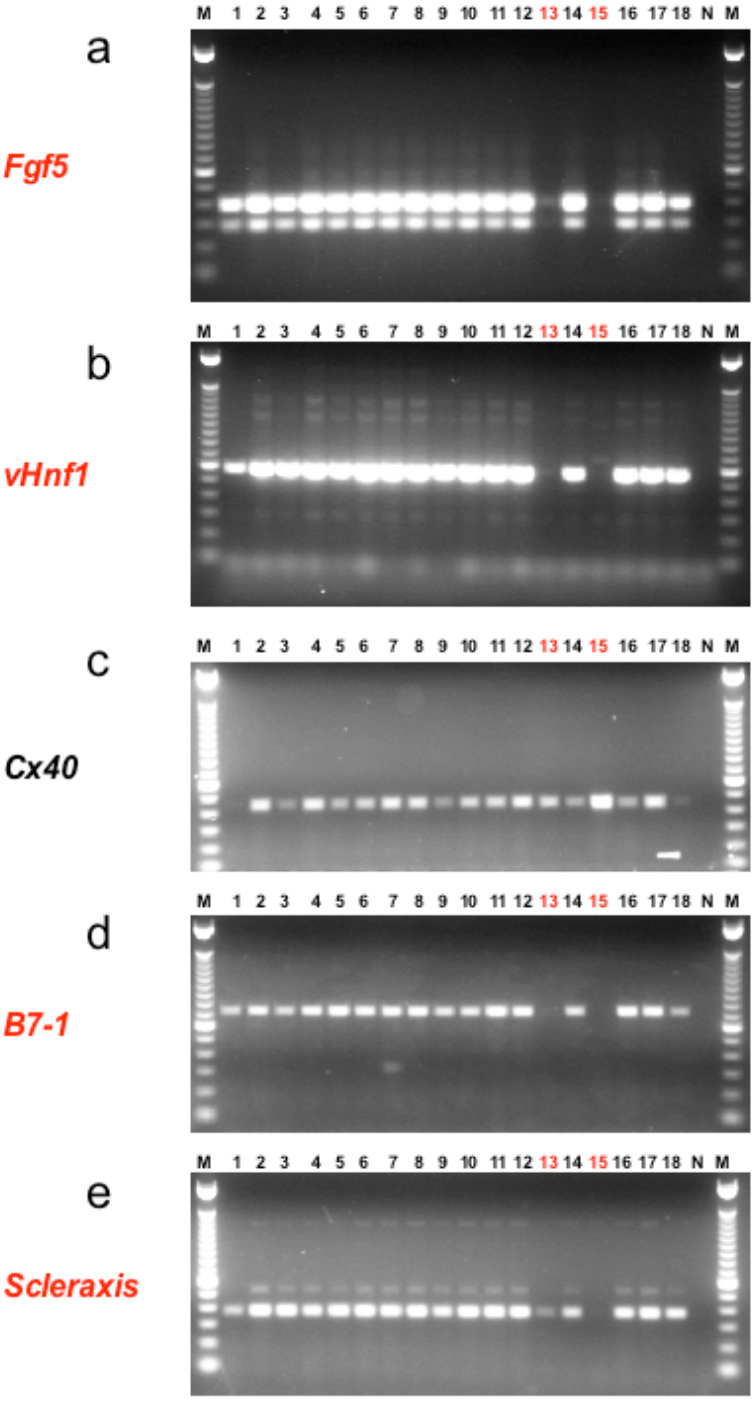
M 1 2 3 4 5 6 7 8 9 10 11 12 13 14 15 16 17 18 N M
a
Fgf5
M 1 2 3 4 5 6 7 8 9 10 11 12 13 14 15 16 17 18 N M
b
vHnf1
M 1 2 3 4 5 6 7 8 9 10 11 12 13 14 15 16 17 18 N M
c
Cx40
M 1 2 3 4 5 6 7 8 9 10 11 12 13 14 15 16 17 18 N M
d
B7-1
M 1 2 3 4 5 6 7 8 9 10 11 12 13 14 15 16 17 18 N M
e
Scleraxis

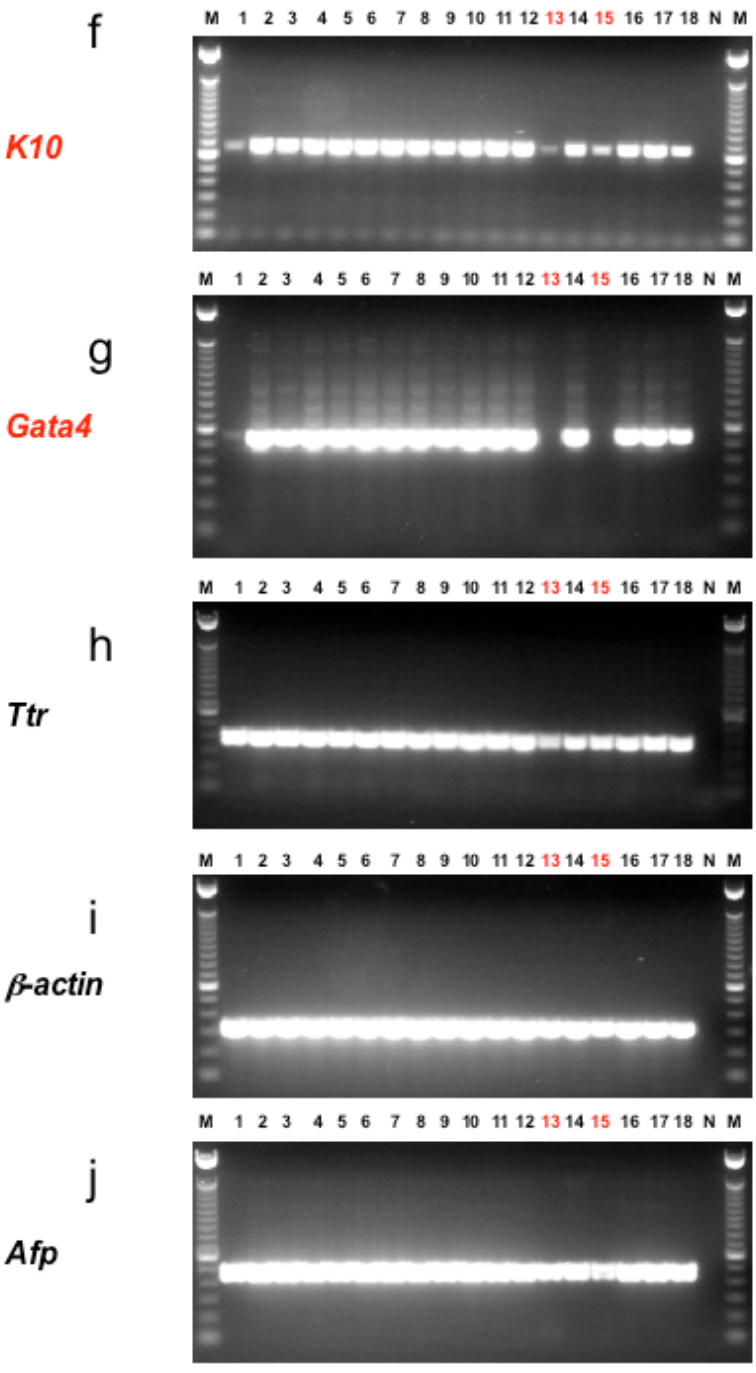
f
K10
M 1 2 3 4 5 6 7 8 9 10 11 12 13 14 15 16 17 18 N M
g
Gata4
M 1 2 3 4 5 6 7 8 9 10 11 12 13 14 15 16 17 18 N M
h
Ttr
M 1 2 3 4 5 6 7 8 9 10 11 12 13 14 15 16 17 18 N M
i
β-actin
M 1 2 3 4 5 6 7 8 9 10 11 12 13 14 15 16 17 18 N M
j
Afp
M 1 2 3 4 5 6 7 8 9 10 11 12 13 14 15 16 17 18 N M

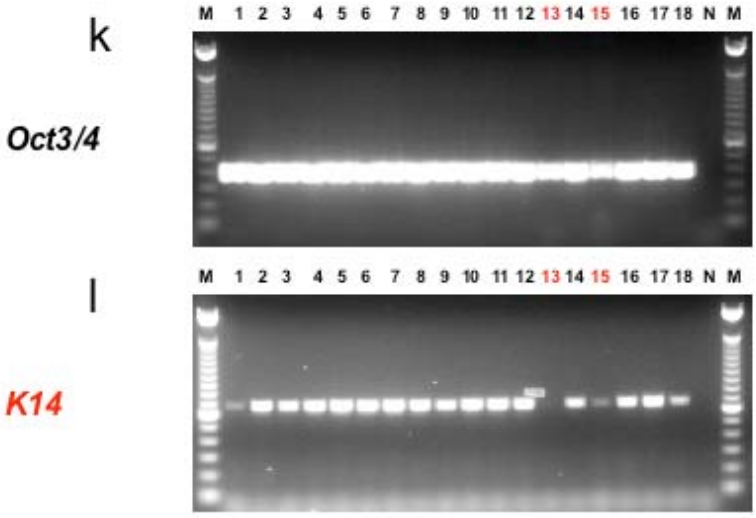

Fig. 5-4 RT-PCR results of Day 8 embryoid bodies. a. *Fgf5*. **b.** *vHnf1*. **c.** *Cx40*. **d.** *B7-1*. **e.** *Scleraxis*. **f.** *K10*. **g.** *Gata4*. **h.** *Ttr*. **i.** *β-actin*. **j.** *Afp*. **k.** *Oct3/4*. **l.** *K14*. Note that lane 13 is WW103-8E6 (marked in red). Lane 1 is the AB2.2 wild type ES cell line. Lane 2 is the WW93-A12 control line, all the other lanes are irrelevant mutant cell lines. At day 8, EBs derived from WW103-8E6 didn't express *Fgf5, vHnf, B7-1, Gata4 and K14*. The expression of *Scleraxis* and *K10* was also down-regulated compared to WW93-A12 control. Markers that are down-regulated are marked in red. Interestingly, the expression of various markers differs between EBs from AB2.2 (lane 1) and those from WW93A12 (lane 2).The expression pattern of the mutant cell lines is more similar to WW93-A12. In the whole screen, WW93A12 and its subclones were used as control.

a

b

c

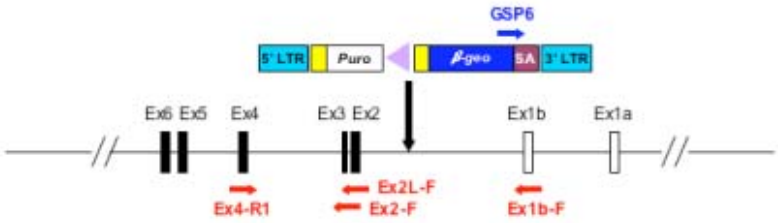
GSP6
5' LTR
Puro
β-geo
SA
3' LTR
Ex6 Ex5
Ex4
Ex3 Ex2
Ex1b
Ex1a
Ex4-R1
Ex2L-F
Ex2-F
Ex1b-F

d

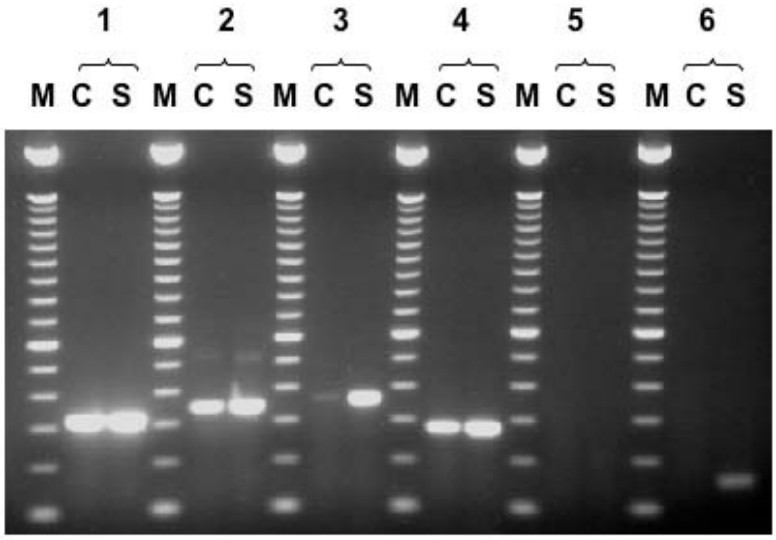
1
2
3
4
5
6
M C S M C S M C S M C S M C S M C S

Fig. 5-5 WW103-8E6. a. Splinkerette PCR result. *Spe*I/*Xba*I/*Nhe*I Splinkerette PCR product mapped the proviral insertion site to the first intron of the *Pecam* gene. The second and the third exons of *Pecam a*re marked in red, and the splinkerette PCR fragment is marked in blue. **b.** 5'RACE result. The 5' RACE product was mapped to an alternative exon of *Pecam*.The splice acceptor of the SA-βgeo cassette is marked in black, the *Pecam* alternative exon 1b is marked in red, the polyC tail is marked in green. **c.** Schematic illustration of the proviral insertion in WW103-8E6. *Pecam* gene specific primers were designed to decide the structure of the clone. PECAM-Ex1b-F, PECAM-Ex2L-F, PECAM-Ex2-F and PECAM-Ex4-R1 primers are shown as red arrows, SA-βgeo cassette specific primer GSP6 is shown as a blue arrow, the coding exons are marked in black. **d.** RT-PCR result. 1: positive control, *β-actin* RT primers; 2: PECAM-Ex1b-F/PECAM-Ex4-R1; 3: PECAM-Ex2L-F/PECAM-Ex4-R1; 4: PECAM-Ex2-F/PECAM-Ex4-R1; 5: negative control, no primers were added. 6: PECAM-Ex1b-F/GSP6. M, 100 bp ladder (Invitrogen); C: RNA extracted from undifferentiated WW93-A12 ES cells; S: RNA extracted from undifferentiated WW103-8E6 ES cells. Note that in undifferentiated WW93-A12 ES cells, most *Pecam* transcripts start from Exon 1b. In undifferentiated WW103-8E6 ES cells, a large portion of Pecam transcripts start from Exon 2. But significant amount of transcripts started from Exon 1b were still detected.

a

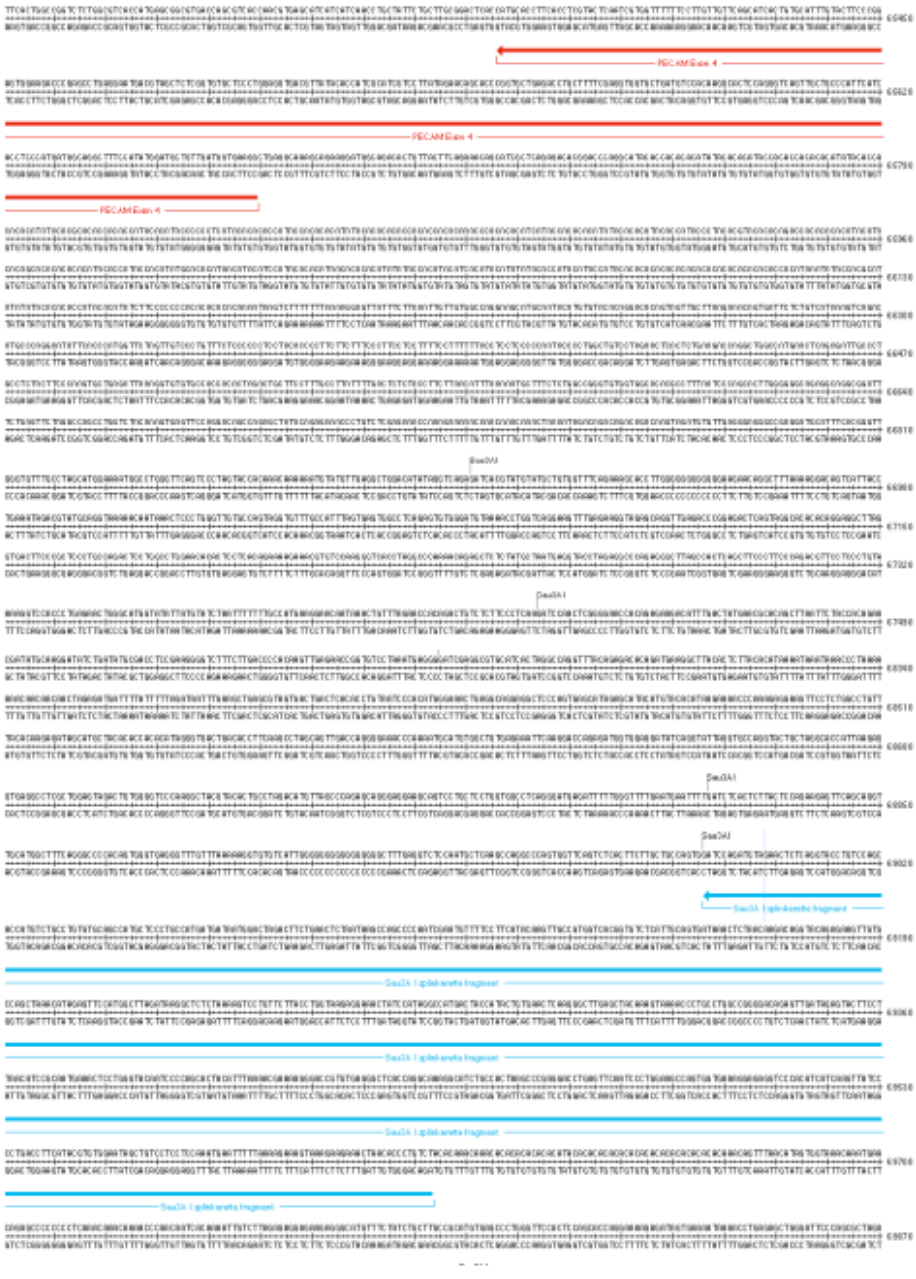
PECAM Exon 4
PECAM Exon 4
PECAM Exon 4
Sau3AI
Sau3AI
Sau3AI
Sau3A I gDNA enrich fragment
Sau3A I gDNA enrich fragment
Sau3A I gDNA enrich fragment
Sau3A I gDNA enrich fragment

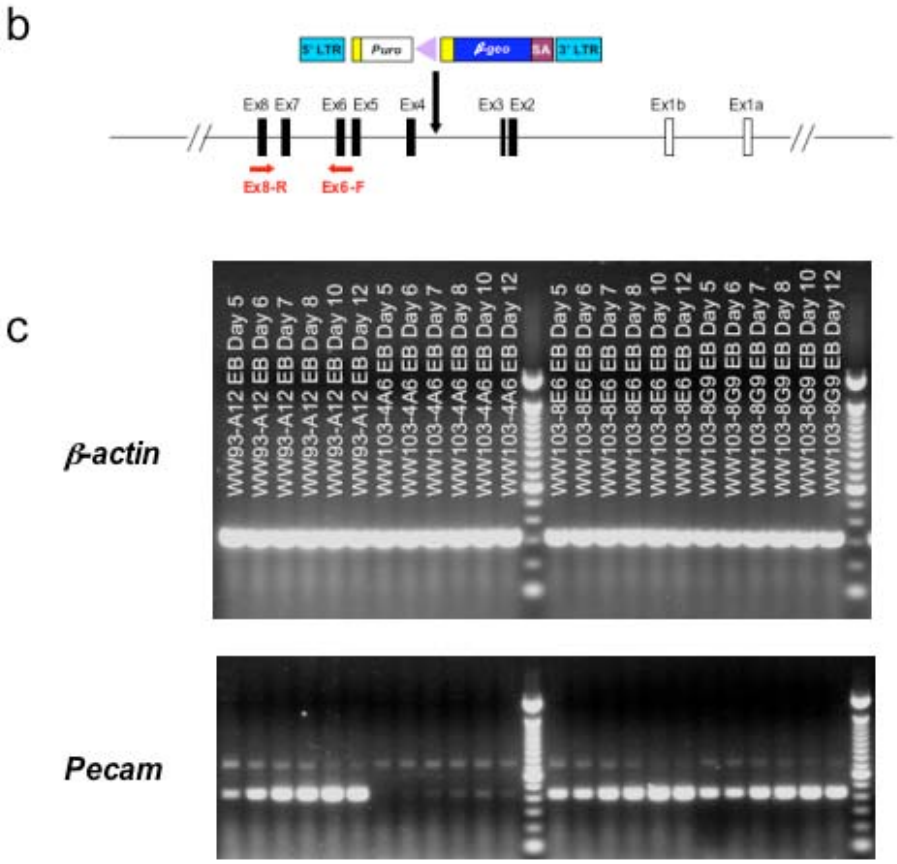

Fig. 5-6 WW103-4A6. a. Splinkerette PCR result. *Sau*3AI Splinkerette PCR product mapped the proviral insertion site to the third intron of the *Pecam* gene. The forth exon of *Pecam* is marked in red, and the splinkerette PCR fragment is marked in blue. **b.** Schematic illustration of the proviral insertion in WW103-4A6. *Pecam* gene specific primers were designed to confirm the structure of the allele. PECAM-Ex6-F and PECAM-Ex8-R primers are shown as red arrows, the coding exons are marked in black. **c.** RT-PCR result. The expression of *Pecam* during *in vitro* differentiation of WW93-A12, WW103-4A6, WW103-8E6 and WW103-8G9 was examined by RT-PCR using PECAM-Ex6-F and PECAM-Ex8-R primers. Note that the *Pecam* expression was completely blocked in WW103-4A6, but not in WW103-8E6 and WW103-8G9.

In an attempt to resolve how this situation could have occurred, Southern analysis was performed using a *Pecam* specific probe (Fig. 5-7). This revealed that both WW103-8E6 and WW103-8G9 were heterozygous for *Pecam* locus. But interestingly, the ratio between the targeted restriction fragment and the wild-type restriction fragment is not 1:1. For WW103-8E6, the ratio is around 2:1, while for WW103-8G9 the ratio is around 1:2. The unexpected Southern result suggested that both clones might be trisomic. If so, it is most likely that the trisomy appeared after the end point cassette targeting and before the retrovirus infection. In this case, the original trisomy would contain two 3' *Hprt* chromosomes targeted with the end point cassette, and one 5' *Hprt* wild-type chromosome. After regional trapping, the puromycin resistant trisomy will have one 3' *Hprt* chromosome with an inversion, one 3' *Hprt* chromosome with targeted end point cassette and one 5' *Hprt* wild-type chromosome. Induced mitotic recombination can generate two different products: clones with two inversion chromosomes and one chromosome with the end point cassette (WW103-8E6), or clones with one inversion chromosome and two chromosomes with the end point cassette (WW103-8G9). In both cases, the clones will carry three targeted E_2DH alleles (end point targeting), thus Southern analysis using E_2DH probe can not distinguish these trisomies from the homozygous inversion clones.

Therefore the impaired differentiation potential of WW103-8E6 does not have any direct connection with the *Pecam* trapping and the subsequent inversion. This may be the result of the up-regulation of the chromosome 11 genes caused by the extra chromosome.

5.2.4 WW103-14F11 (*2810410L24Rik*)

As described in the previous chapter, the WW103-14F11 subclone has a proviral insertion at the *2810410L24Rik* locus (119.9 Mb) (Fig. 5-8a), which is close to the telomere of the chromosome 11. But instead of trapping the *2810410L24Rik* gene, which is transcribed from the sense strand (from centromere to telomere), the retrovirus trapped another transcript transcribed from the anti-sense strand (from telomere to centromere), *D030042H08Rik*.

a

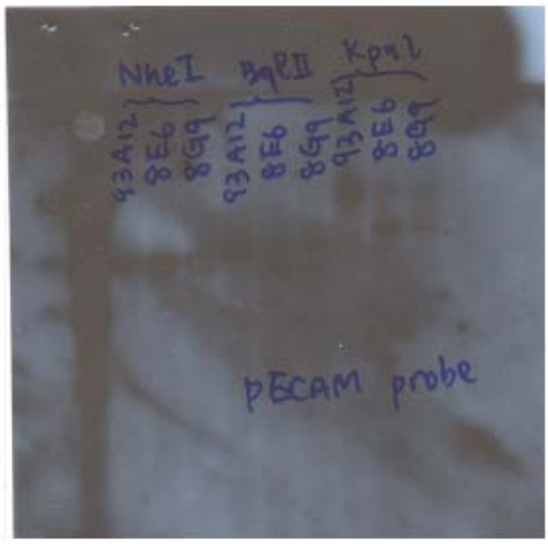
NheI
BglII
KpnI
93A12
8E6
8G9
93A12
8E6
8G9
93A12
8E6
8G9
pECAM probe

b

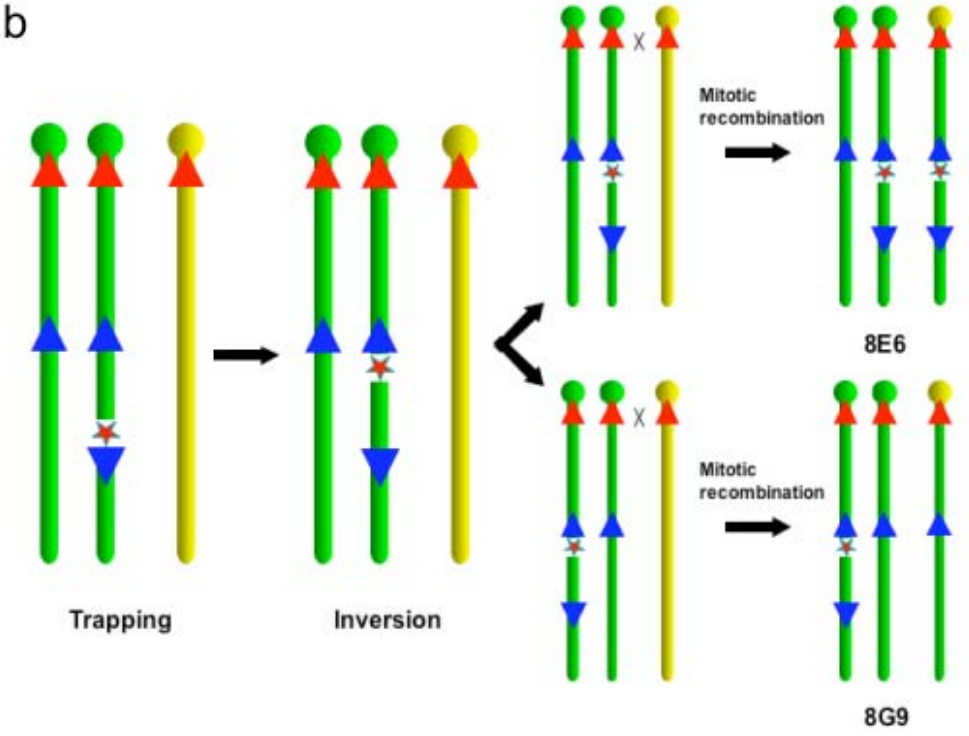
Trapping
Inversion
Mitotic recombination
8E6
Mitotic recombination
8G9

Fig. 5-7 WW103-8E6 and 8G9 are both chromosome 11 trisomies. a. Southern analysis of clones, WW103-8E6 and WW103-8G9. A *Pecam* specific probe was used to detect a 10.6 kb *Bgl*II wild type fragment and a 9 kb *Bgl*I targeted fragment. The same probe was also used to detect a 30 kb *Kpn*I wild type fragment and a 19 kb targeted fragment. Both WW103-8E6 and WW103-8G show a wild type fragment for both digestions. But the ratio between the targeted restriction fragment and the wild type restriction fragment is not 1:1. For WW103-8E6, the ratio is around 2:1, while for WW103-8G9 the ratio is around 1:2. The Southern result suggested that both clones might be trisomic. **b.** A schematic illustration of possible recombination in WW103-8E6 and WW103-8G. The original trisomy probably contained two 3' *Hprt* chromosomes targeted with the end point cassette, and one 5' *Hprt* wild type chromosome. After regional trapping, the puromycin resistant trisomy has one 3' *Hprt* chromosome with the inversion, one 3' *Hprt* chromosome with the end point cassette and one 5' *Hprt* wild type chromosome. Induced mitotic recombination can generate two different products, depending on which 3' *Hprt* chromosome participates in the recombination process. Clones can be generated with two inversion chromosomes and one chromosome with the targeted end point cassette (WW103-8E6), or clones with one inversion chromosome and two chromosomes with the targeted end point cassette (WW103-8G9).

a

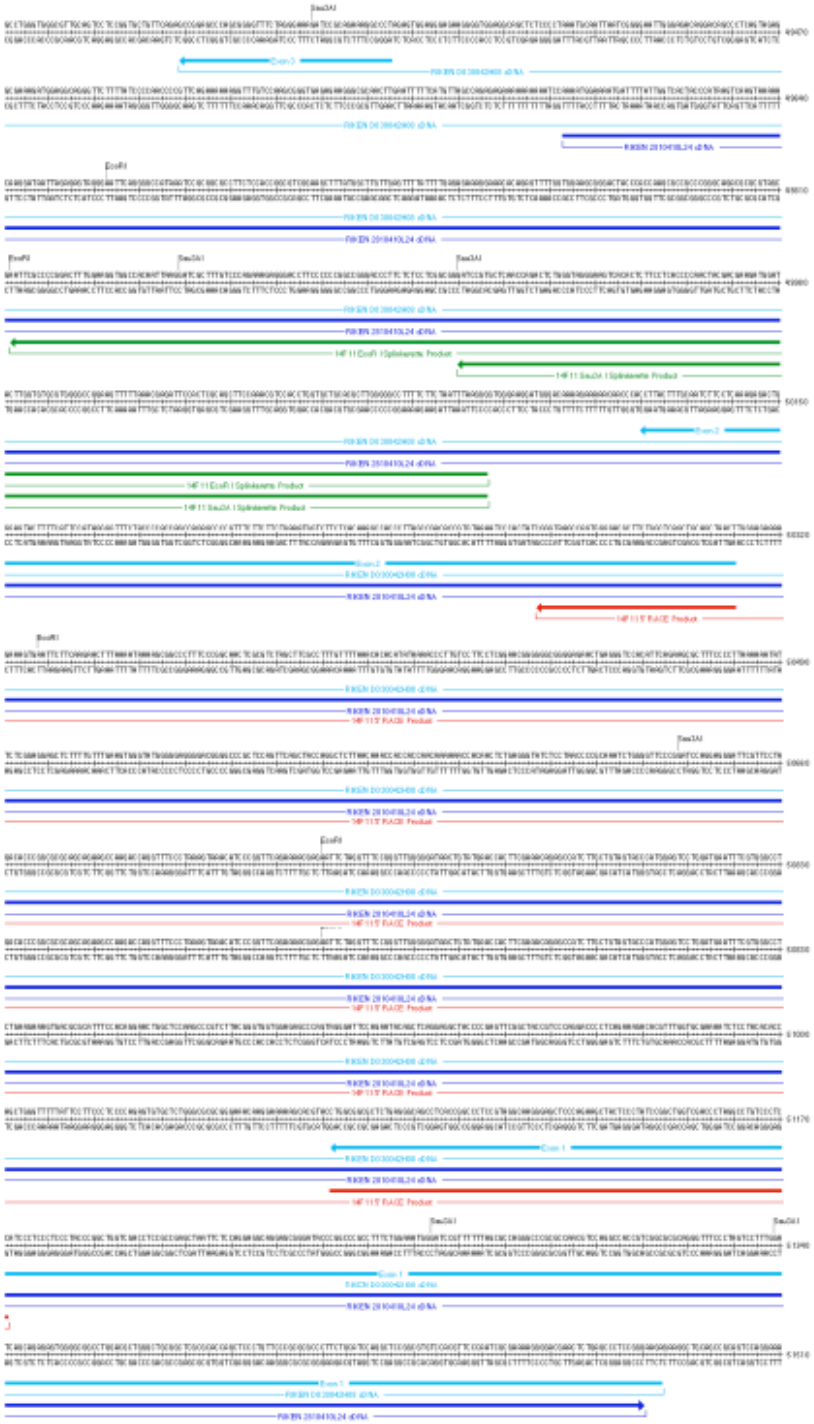

b

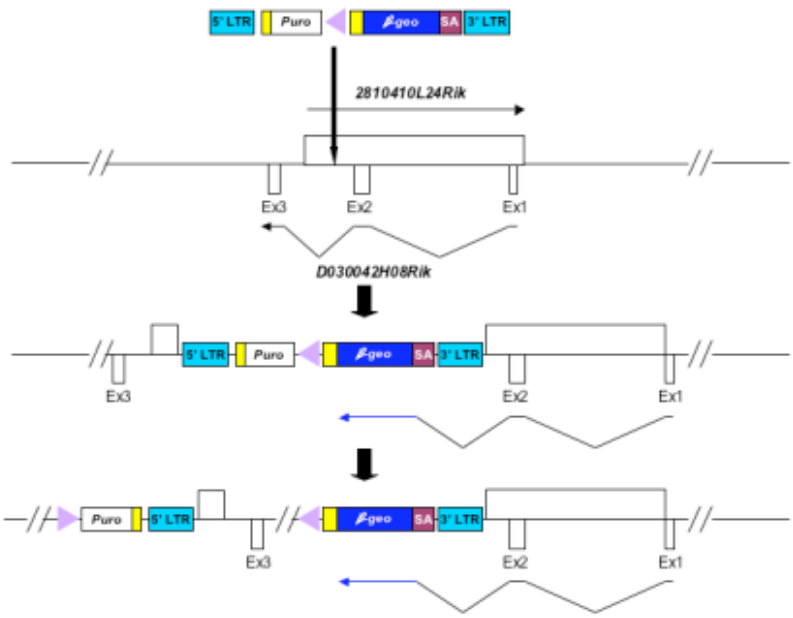
5' LTR
Puro
βgeo
SA
3' LTR
2810410L24Rik
Ex3
Ex2
Ex1
D030042H08Rik

c

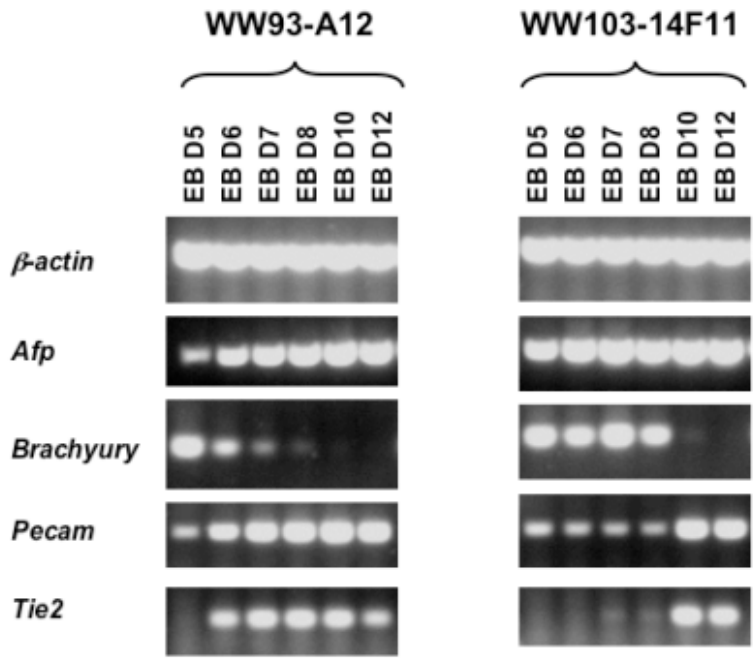
WW93-A12
WW103-14F11
EB D5
EB D6
EB D7
EB D8
EB D10
EB D12
β-actin
Afp
Brachyury
Pecam
Tie2

Fig. 5-8 WW103-14F11. a. Splinkerette PCR and 5' RACE.results. *Eco*RI and *Sau*3AI Splinkerette PCR products have both mapped the proviral insertion site to the *2810410L24Rik* locus. The 5' RACE result matched another transcript *D030042H08Rik*.The *2810410L24Rik* transcript is marked in dark blue, the *D030042H08Rik* transcript is marked in light blue, the splinkerette PCR fragments are marked in green and the 5'RACE product is marked in red. **b.** Schematic illustration of the structure of proviral insertion and the subsequent inversion in WW103-14F11. **c.** RT-PCR results of EBs derived from WW013-14F11 and WW93-A12. Note that *Pecam* and *Tie2* RT-PCR results showed that the up-regulation of these two markers in the differentiation process was significantly delayed. On the other hand, the early mesoderm marker, *Brachyury*'s down-regulation was also delayed.

The splinkerette results mapped the proviral insertion site between the second and third exons of *D030042H08Rik*. However, the 5' RACE result did not match the *D030042H08Rik* cDNA sequence perfectly, although the transcript structure is similar. It is possible that the 5' RACE result and the *D030042H08Rik* cDNA sequence represent two different alternative splice forms of the same gene.

Nevertheless, the gene-trap retrovirus insertion and the subsequent inversion will disrupt the transcripts from both strands (Fig. 5-8b). The *in vitro* differentiation results showed that EBs derived from WW103-14F11 have impaired potential to develop into endothelial cells. RT-PCR using *Pecam* and *Tie2* primers has shown that the up-regulation of the expression of these two markers during the differentiation process was significantly delayed. On the other hand, the early mesoderm marker, *Brachyury*'s down-regulation was also delayed (Fig. 5-8c).

Further confirmation of this subclone is still undergoing. One way to directly confirm the defective endothelial cell differentiation is to use collagen IV coated dishes to induce undifferentiated ES cells to first differentiate into $Flk1^+$ cells (Yamashita, Itoh et al. 2000). When FACS sorted $Flk1^+$ cells were cultured with the addition of VEGF, these cells will further differentiate into PECAM1+ sheets of endothelial cells, which also express other endothelial cell-specific markers, such as *VE-cadherin* and *CD34*. By comparing the endothelia cell differentiation of the WW103-14F11 cells and the wild-type control cells, it will be possible to identify the molecular mechanism underlying the defective phenotype and determine at which stage the differentiation into endothelial lineage is blocked. However, it will be difficult to distinguish the phenotypes of the two genes transcribed from the opposite directions.

5.2.5 WW103-13D10 (*LOC217071*)

*Sau*3A1 and SpeI/*Xba*I/*Nhe*I Splinkerette PCR products mapped the proviral insertion site in the WW103-13D10 clones to the second intron of a hypothetical mouse gene, *LOC217071* (Fig. 5-9a and b). This gene is transcribed from the sense strand (from the centromere to telomere), and

Southern analysis using an *E_2DH* 3' probe has confirmed that this clone is homozygous for the targeted *E_2DH* allele. Southern analysis using a *LacZ* probe has shown that it only carried a 6.9 kb *Kpn*I restriction fragment which suggested that WW103-13D10 contains an intact proviral insertion. As discussed in the previous chapter, this might be caused by a G2 *trans* recombination event. The duplication chromosome has both a functional *Puro* and a functional *Bsd* cassette, and it can become homozygous after induced mitotic recombination because it has not lost any genetic material.

The homozygous duplication clone showed an obvious abnormality in *in vitro* differentiation. The undifferentiated WW103-13D10 ES cells expressed high levels of markers for differentiated cell types, such as *Afp*, *Gata4* and *Hnf4*. The expression of undifferentiated ES cell markers, like *Nodal* and *Oct3/4*, was significantly down-regulated, compared to the WW93-A12 control (Fig. 5-9c).

Interestingly, during the process of differentiation, the EBs made from WW103-13D10 ES cells seemed to differentiate normally. At day 5, they lost the expression of *Afp*, but regained the expression of *Nodal* and *Oct3/4*. After this, various markers showed expression patterns similar to those which were observed in the WW93-A12 control. But *Hnf4* and *Gata4* expression were still significantly up-regulated compared to the control.

Sib-selection was carried out on two subclones each from WW93-A12 and WW103-13D10. The same number of undifferentiated ES cells were plated into the wells of a gelatinized 24-well plate and selected in M15, M15+G418, M14+puromycin, M15+blasticidin and M15+HAT, respectively. WW103-13D10 was resistant to both puromycin and blasticidin, which suggested that this clone have two duplication chromosomes, instead of two inversion chromosomes (Fig. 5-9d). Most likely, the phenotype observed in WW103-13D10 was caused by the duplication, instead of the disruption of the *LOC217071* locus.

a

b

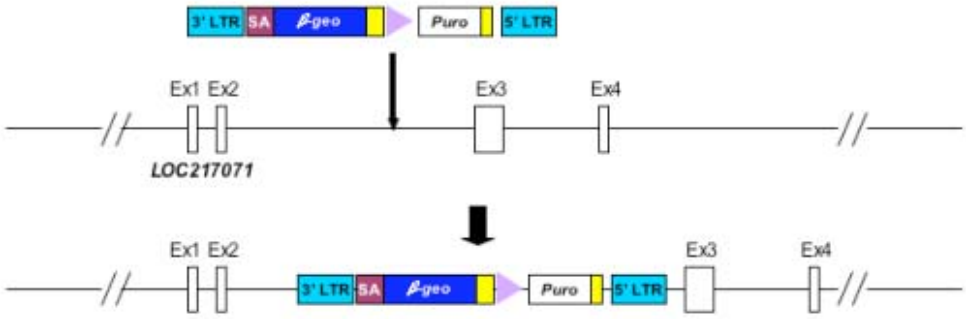
3' LTR
SA
β-geo
Puro
5' LTR
Ex1 Ex2
Ex3
Ex4
LOC217071
Ex1 Ex2
3' LTR
SA
β-geo
Puro
5' LTR
Ex3
Ex4

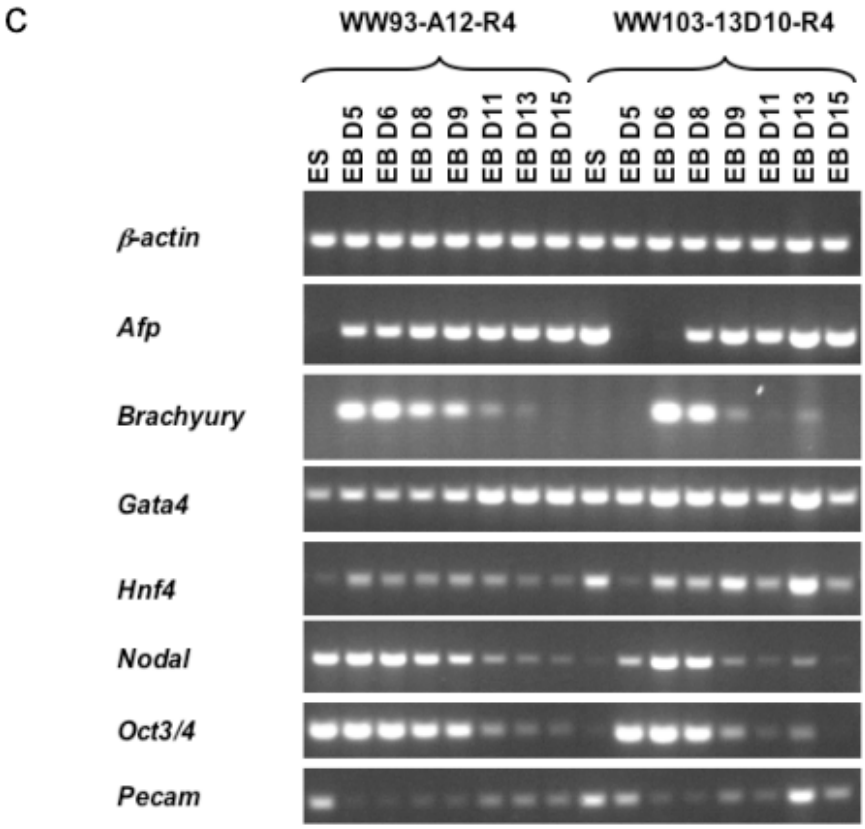
c
WW93-A12-R4
WW103-13D10-R4
ES
EB D5
EB D6
EB D8
EB D9
EB D11
EB D13
EB D15
β-actin
Afp
Brachyury
Gata4
Hnf4
Nodal
Oct3/4
Pecam

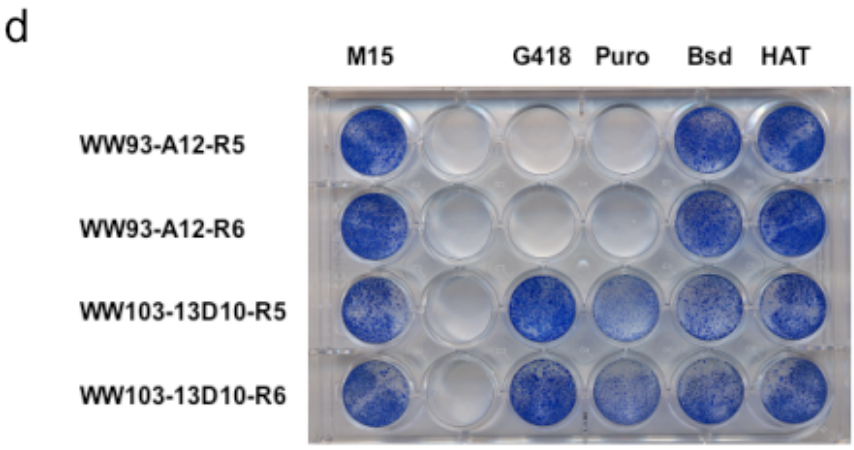
d
M15
G418
Puro
Bsd
HAT
WW93-A12-R5
WW93-A12-R6
WW103-13D10-R5
WW103-13D10-R6

Fig. 5-9 WW103-13D10 a. Splinkerette PCR results. *Spe*I/*Xba*I/*Nhe*I and *Sau*3AI Splinkerette PCR products have mapped the proviral insertion site to the *LOC217071* locus. The splinkerette PCR fragments are marked in green. **b.** Schematic illustration of the structure of proviral insertion in WW103-14F11. **c.** RT-PCR results of EBs derived from WW013-14F11 and WW93-A12. Note undifferentiated WW103-13D10 ES cells express high amounts of *Afp*, *Hnf4* and *Gata4,* but low amount of *Oct3/4* and *Nodal*. Despite the altered expression of these markers,the EBs derived from WW103-13D10 ES cells seem to differentiate normally. **d.** Sib-selection of WW93-A12 and WW103-13D10 clones. Two subclones of each cell line were used for the sib selection. Same amount of undifferentiated ES cells were plated onto a gelatinized 24-well plate and selected with M15, M15+G418, M14+Puromycin, M15+Blasticidine and M15+HAT, respectively. WW103-13D10 was resistant to both Puromycin and Blasticidine, which suggested that this clone is a homozygous duplication, instead of a homozygous inversion.

5.2.6 WW103-18F11 (*Acly*)

One of the mitotic recombination clones, WW103-18F11, showed impaired *in vitro* differentiation potential. After EBs made of WW103-18F11 ES cells were plated on the gelatinized tissue culture plates at Day 5, the EBs did not form cystic three-dimensional structures.

When RT-PCR was performed on RNA extracted from WW103-18F11 embryoid bodies collected at different time points, these EBs were found to express high levels of the undifferentiated ES cell markers, *Oct3/4* and *Nodal*, as late as Day 18 of the *in vitro* differentiation protocol. The expression of *Oct3/4* and *Nodal* still decreased a little during the differentiation process, but down-regulation was not as rapid as that in the control cell line (Fig. 5-10a and e).

Tie2 expression was not detected during the whole process of differentiation of WW103-18F11 cells. The expression of *Pecam* was maintained at a constant basal level, instead of being up-regulated, as was observed in the WW93-A12 control cell line (Fig. 5-10b). Both of the markers are endothelial cell-specific proteins expressed during the formation of vascular structures in ES-derived EBs. The *Tie2* gene encodes a growth factor receptor, while the *Pecam* protein is an endothelial cell specific antigen. Vittet *et al*. (1996) has shown that both genes are expressed at low levels in undifferentiated ES cells. Normally, in the process of *in vitro* differentiation, the expression of both genes is absent at day 0-3 and is detected again from day 4. After this, the expression level of both genes is consistently up-regulated, as detected by Northern blotting and/or Immunofluorescence. However, in that experiment, only EBs from Day 3 to Day 7 were checked (Vittet, Prandini et al. 1996). In my experiment, I have observed the expression of *Tie2* and *Pecam* in the control line throughout the 15-day differentiation process. Thus, my observation suggested that the differentiation of endothelial cells in the mutant cell line was significantly impaired over the entire 15-day differentiation process.

The expression pattern of the early mesodermal markers (*Bmp4*, *Brachyury*, *Goosecoid*) is similar between WW103-18F11 and WW93-A12 (Fig. 5-10c). However, low levels of expression of *Brachyury* and *Goosecoid* were still detected in WW103-18F11 derived EBs collected at later stages of the differentiation process, while no expression of these markers were detected in later stage EBs derived from WW93A12. The expression of one of the endodermal markers, *Hnf4*, in WW103-18F11 was much lower than that in the control. Apart from these changes, no major differences were observed in the levels of expression of the other markers (Fig. 5-10d).

5' RACE results revealed that the gene-trap retrovirus trapped Exon 1 of ATP-citrate lyase (*Acly*) (Fig. 5-11a). *Acly* is one of two cytosolic enzymes in eukaryotes that synthesize acetyl-coenzyme A (acetyl-CoA), the other enzyme is acetyl-CoA synthetase 1. *Acly* catalyzes the formation of acetyl-coenzyme A (CoA) from citrate and CoA, and hydrolyzes ATP to ADP and phosphate. Because acetyl-CoA is an essential component for cholesterol and triglycerides synthesis, *Acly* is believed to be a potential therapeutic target for hyperlipidemias ad obesity (Beigneux, Kosinski et al. 2004).

To characterize this mutant cell line further, pure subclones of WW103-18F11 were derived by low density plating to form single colonies. Six subclones were picked and expanded. To confirm chromosomal structure of these subclones, sib-selection was performed on two of the WW103-18F11 subclones, WW103-18F11-R1 and WW103-18F11-R6, as well as two subclones of the control cell line, WW93-A12-R4 and WW93-A12-R5. An equal number of ES cells from each subclone were plated onto multiple 6-well plates and selected with M15, M15+puromycin, M15+blasticidin, M15+G418 and M15+HAT, respectively. As expected, the two WW103-18F11 subclones are $Puro^R$, Neo^R, Bsd^S and HAT^R, and the two WW93-A12 subclones are $Puro^S$, Neo^S, Bsd^R and HAT^R. The drug resistance pattern of WW103-18F11 suggests that WW103-18F11 have undergone correct recombination (Fig. 5-11b).

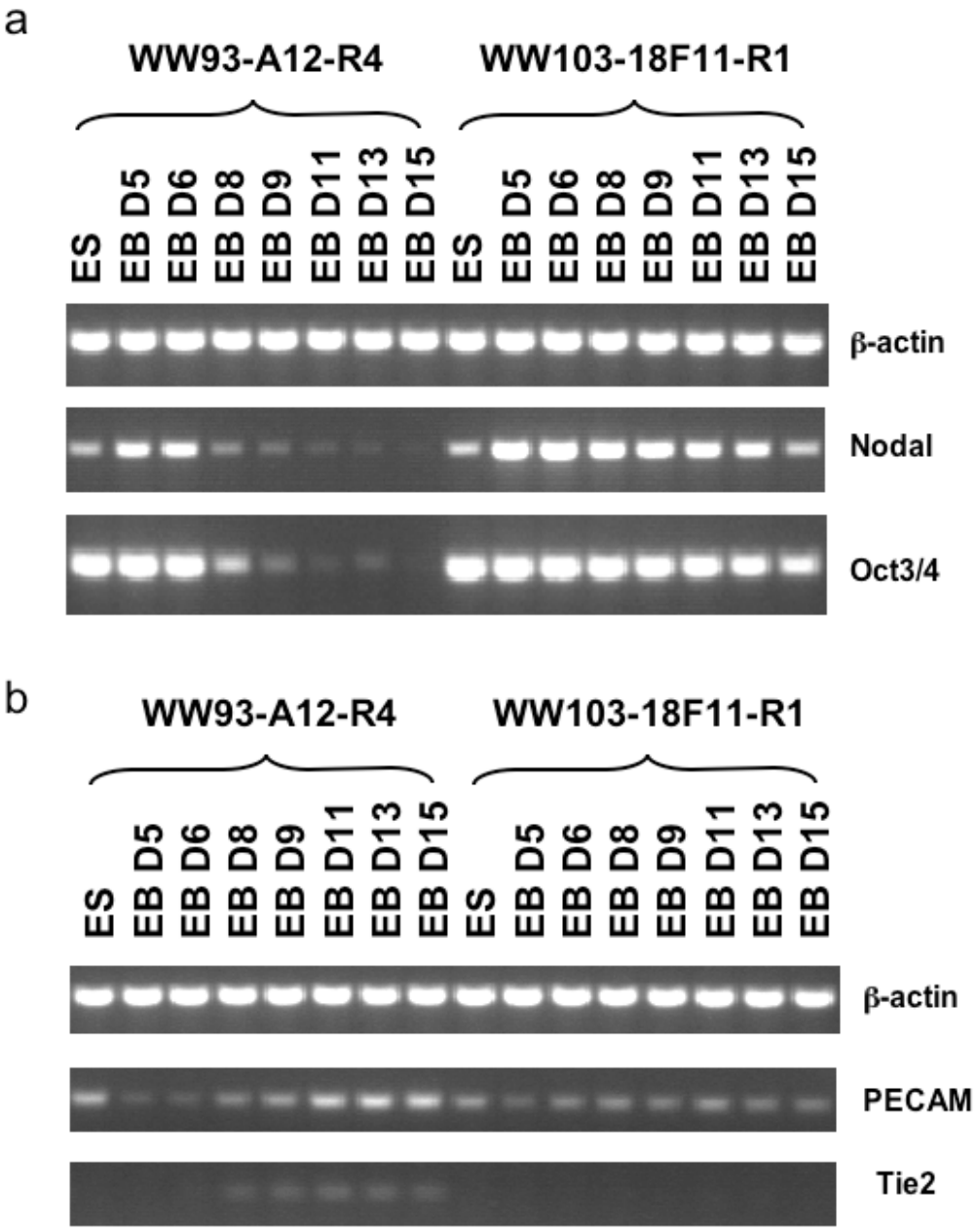
a
WW93-A12-R4
WW103-18F11-R1
ES
EB D5
EB D6
EB D8
EB D9
EB D11
EB D13
EB D15
β-actin
Nodal
Oct3/4
b
WW93-A12-R4
WW103-18F11-R1
ES
EB D5
EB D6
EB D8
EB D9
EB D11
EB D13
EB D15
β-actin
PECAM
Tie2

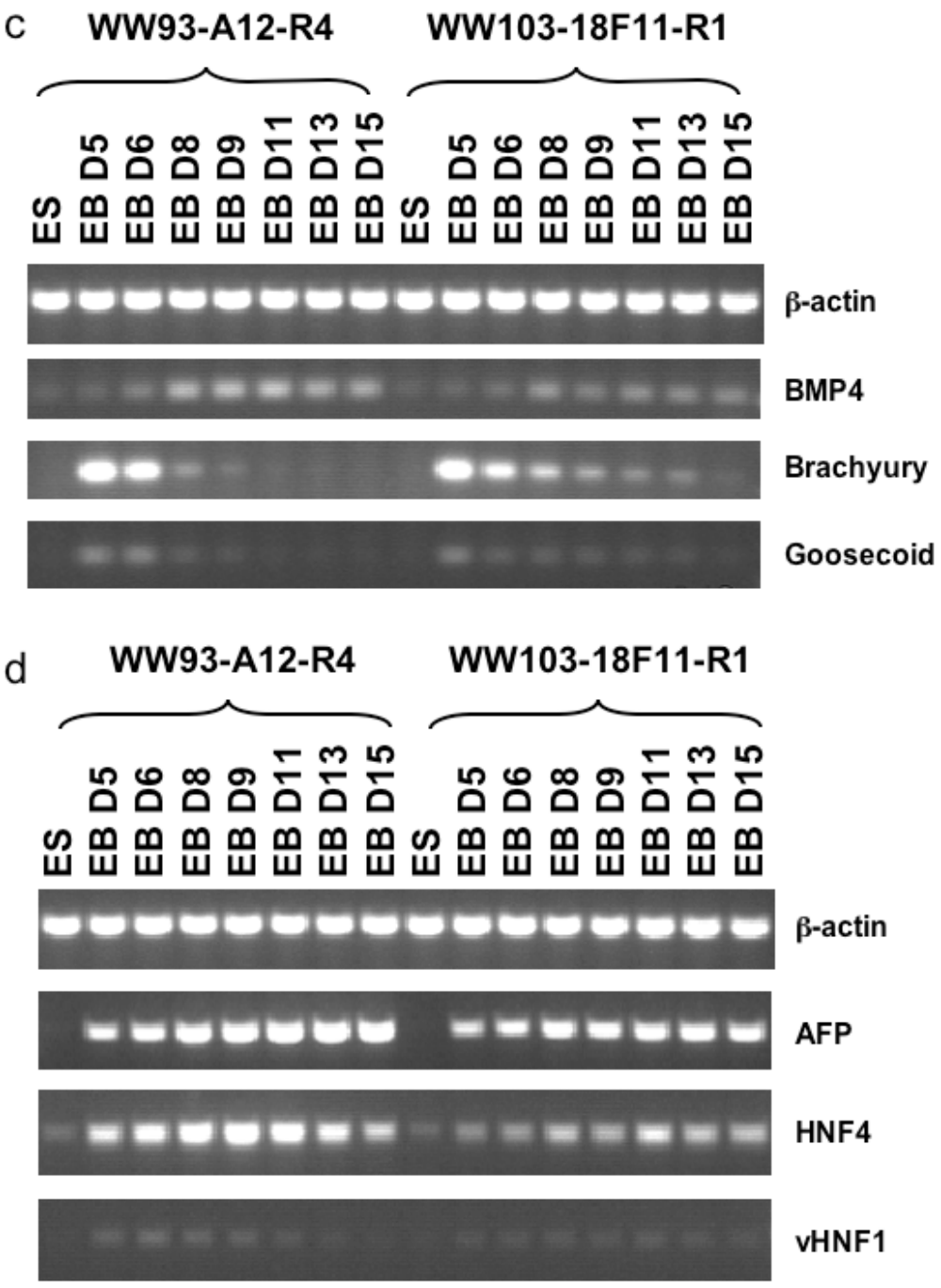
c
WW93-A12-R4
WW103-18F11-R1
ES
EB D5
EB D6
EB D8
EB D9
EB D11
EB D13
EB D15
β-actin
BMP4
Brachyury
Goosecoid
d
WW93-A12-R4
WW103-18F11-R1
ES
EB D5
EB D6
EB D8
EB D9
EB D11
EB D13
EB D15
β-actin
AFP
HNF4
vHNF1

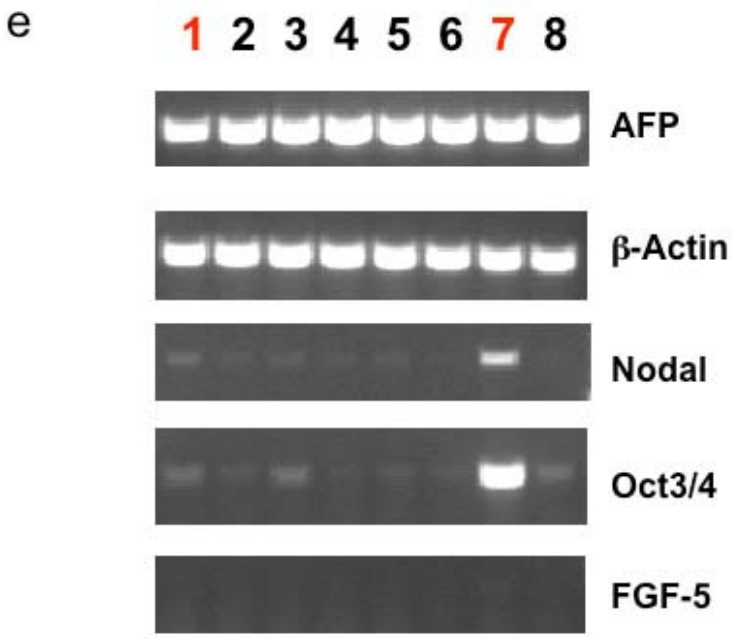

Fig. 5-10 RT-PCR results of WW103-18F11. a. Primitive ectoderm markers. The expression of *Oct3/4* and *Nodal* decreased slightly in the differentiation process. **b.** Endothelial markers. *Tie2* expression was not detected throughout the differentiation process of WW103-18F11 cells. The expression of *Pecam* was not up-regulated as observed in WW93-A12 control cell line. **c.** Early mesoderm markers. Low levels of expression of *Brachyury* and *Goosecoid* were still detected in WW103-18F11 derived EBs collected at later stages of the differentiation process, while no expression of these markers were detected in later stage EBs derived from WW93A12. **d.** Endoderm markers. The expression of most endoderm markers appears quite similar between the two cell lines. However, the expression of *Hnf4* in WW103-18F11 was much lower than that in the control. **e.** Day 18 embryoid bodies RT-PCR results. Note that WW103-18F11 EBs still express high amount of *Nodal* and *Oct3/4* at day 18. Lane 1, WW93-A12 control cell line; lane 7, WW103-18F11. Lanes 2-6 and 8 are day 18 EBs derived from other irrelevant mutant cell lines.

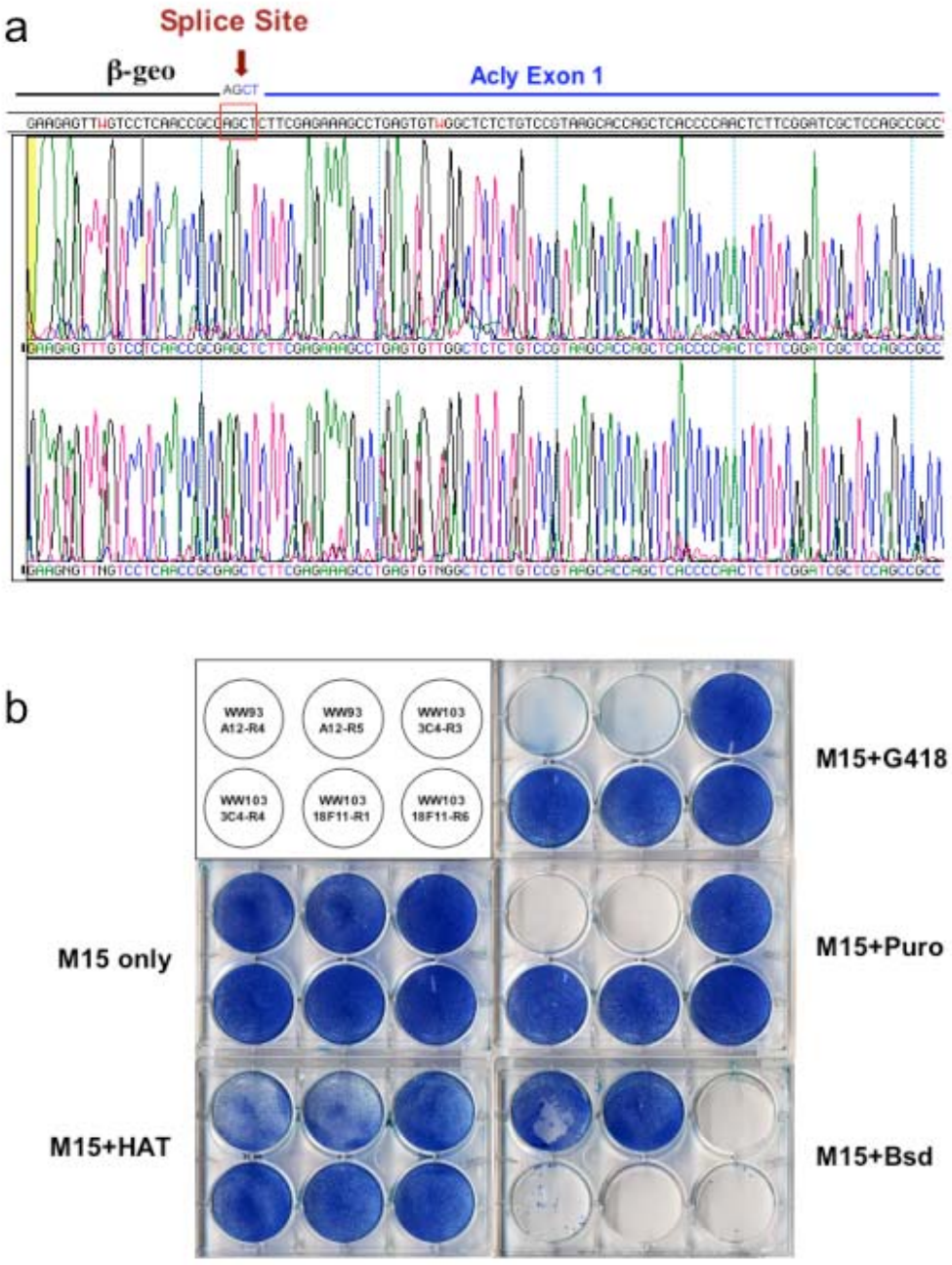
a
Splice Site
β-geo
AGCT
Acly Exon 1
b
WW93 A12-R4
WW93 A12-R5
WW103 3C4-R3
WW103 3C4-R4
WW103 18F11-R1
WW103 18F11-R6
M15+G418
M15 only
M15+Puro
M15+HAT
M15+Bsd

c

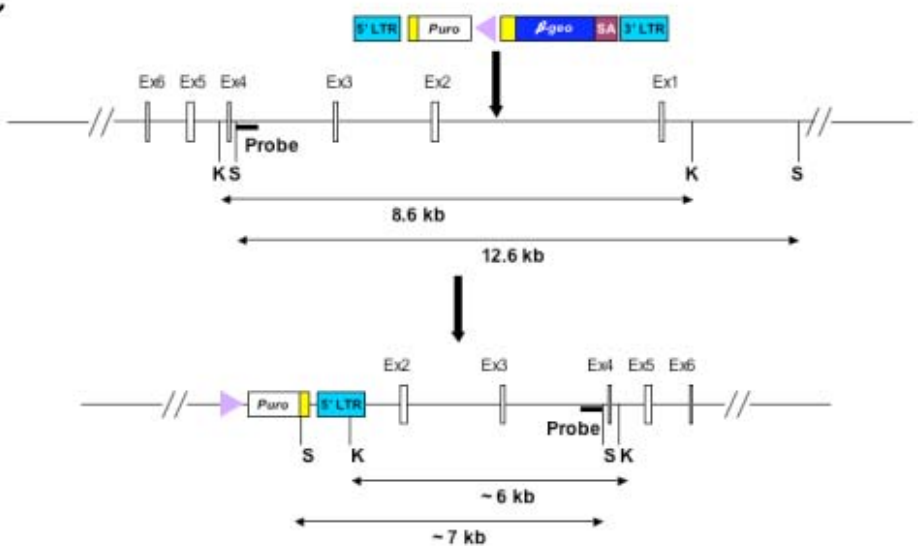
5' LTR
Puro
βgeo
SA
3' LTR
Ex6
Ex5
Ex4
Ex3
Ex2
Ex1
Probe
K S
K
S
8.6 kb
12.6 kb
Puro
5' LTR
Ex2
Ex3
Ex4
Ex5
Ex6
Probe
S
K
S K
~ 6 kb
~ 7 kb

d

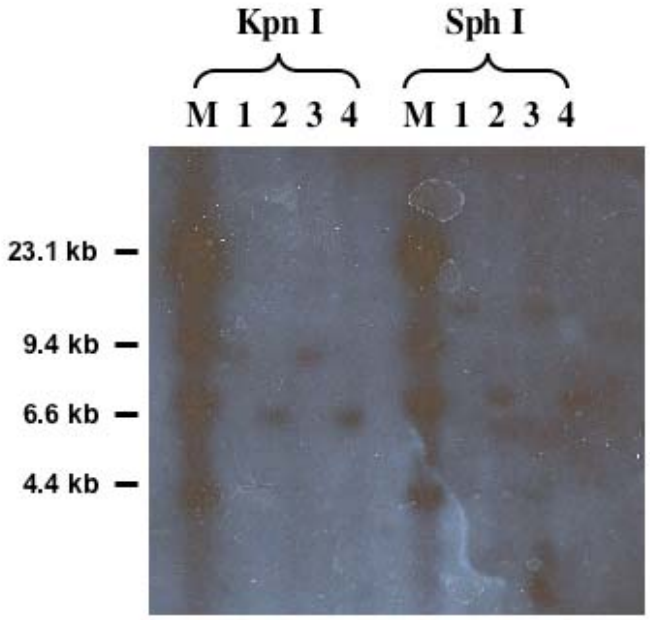
Kpn I
Sph I
M 1 2 3 4
M 1 2 3 4
23.1 kb
9.4 kb
6.6 kb
4.4 kb

Fig. 5-11 Identification of WW103-18F11. a. 5' RACE result. The sequence of the 5' RACE product matched the first exon of *Acly* gene. **b.** Sib-selection of WW103-18F11 and WW93-A12. Sib-selection was carried out on two of the WW103-18F11 subclones, WW103-18F11-R1 and WW103-18F11-R6, as well as two subclones of control cell line, WW93-A12-R4 and WW93-A12-R5. The same number of ES cells from two subclones each of WW93-A12 and WW103-18F11 were plated onto gelatinized 6-well plates and selected with M15, M15+Puromycin, M15+Blasticidine, M15+G418 and M15+HAT, respectively. The two WW103-18F11 subclones are $Puro^R$, Neo^R, Bsd^S and HAT^R, and the two WW93-A12 subclones are $Puro^S$, Neo^S, Bsd^R and HAT^R. The drug resistance pattern of WW103-18F11 suggested that it is a homozygous inversion clone. **c.** Schematic illustration of the structure of the proviral insertion and the subsequent inversion in WW103-18F11. **d.** Southern analysis of WW103-18F11. Southern analysis has been carried out using an *Acly* gene specific probe. This probe can detect an 8.6 kb *Kpn*I restriction fragment for the wild type allele. For WW103-18F11, the probe only detected an 6 kb *Kpn*I restriction fragment for the gene trap allele. Also, the probe only detected an 7 kb *Sph*I restriction fragment for the gene trap allele, instead of the 12.6 kb *Sph*I restriction fragment for the wild type allele. This Southern result has confirmed that both *Acly* alleles have been disrupted by the gene trap insertion. M, λ *Hin*dIII marker (New England Biolabs); lane 1, WW93-A12-R4; lane 2, WW103-18F11-R1; lane 3, WW93-A12-R5; lane 4, WW103-18F11-R6.

Southern analysis was carried out using an *Acly* gene specific probe. When this probe was hybridized to *Kpn*I digested genomic DNA, it detects an 8.6 kb wild-type fragment and an approximately 7 kb gene-trap fragment. When this probe was hybridized to *Sph*I digested genomic DNA, it detects a 12.6 kb wild-type fragment and an approximately 8 kb gene-trap fragment. As expected, only the gene-trap fragment was detected in the WW103-18F11 subclones. This Southern result confirms that both alleles of the *Acly* gene have been disrupted by the gene-trap insertion.

To see whether the gene-trap insertion and the subsequent inversion has disrupted transcription of the locus, PCR primers were used to specifically amplify cDNA fragments from Exon 1 to Exon 2 (F1/R1 and F2/R1) and Exon 1 to Exon 3 (F1/R2 and F2/R2). First strand cDNA was synthesised using total RNA extracted from WW103-18F11 and WW93-A12 ES cells. The RT-PCR results showed that transcription from Exon 1 to downstream exons was blocked. Weak PCR bands were detected for the *Acly*-deficient cell lines, which are likely to be contamination from feeder cells (Fig. 5-12a). Primer pairs F1/GSP4 and F2/GSP4 were used to specifically amplify the Exon 1/β-geo fusion transcript from the trapped allele. As expected, specific bands were only detected for WW103-18F11 subclones, but not for WW93-A12 control (Fig. 5-12c).

To see whether the gene-trap insertion and the subsequent inversion has affected the transcription of downstream exons, PCR primers were designed to specifically amplify cDNA fragments from Exon 24 to Exon 28 (F3/R3 and F3/R4) and Exon 25 to Exon 28 (F4/R3 and F4/R4). Specific PCR bands were detected in the WW103-18F11 mutant cell line and the WW93-A12 control cell line. Therefore it is likely that there is an alternative transcription start point between the retroviral insertion point and Exon 24, but the precise location of the mutant transcript start in WW103-18F11 is not known (Fig. 5-12b).

These RT-PCR primer pairs have also been used to check *Acly* expression during *in vitro* differentiation. In the WW93-A12 control cell line, *Acly* was highly expressed in undifferentiated ES cells, as well as throughout the whole differentiation process. In the WW103-18F11 mutant cell line, the F1/R1 and F2/R2 primer pairs did not detect the expression of the *Acly* upstream exons during *in vitro* differentiation, but the F3/R2 and F4/R4 primer pairs did detect expression of the *Acly* downstream exons (Fig. 5-12d).

To identify a causal link between the gene-trap insertion and inversion at the *Acly* locus and the severely impaired differentiation potential, a BAC rescue experiment was carried out to reverse the phenotype of the WW103-18F11 ES cell clone. A 129 S7 BAC clone, BMQ-290J5 was identified in Ensembl and confirmed to contain the complete *Acly* gene by PCR (Fig. 5-13a and data not shown). A *PGK-EM7-Bsd-bpA* cassette (pL313) was inserted into the *SacB* gene on the backbone of this BAC clone by *E. coli* recombination (Liu, Jenkins et al. 2003). The correct insertion of the *Bsd* cassette into the BAC backbone was confirmed by Southern using a *SacB* specific probe (Fig. 5-13b and c).

a

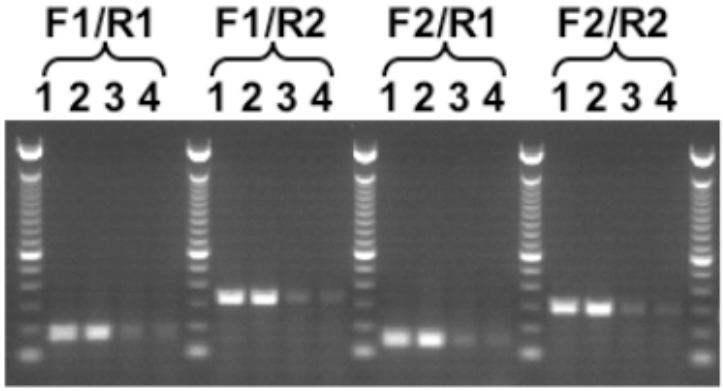
F1/R1
F1/R2
F2/R1
F2/R2
1 2 3 4
1 2 3 4
1 2 3 4
1 2 3 4

b

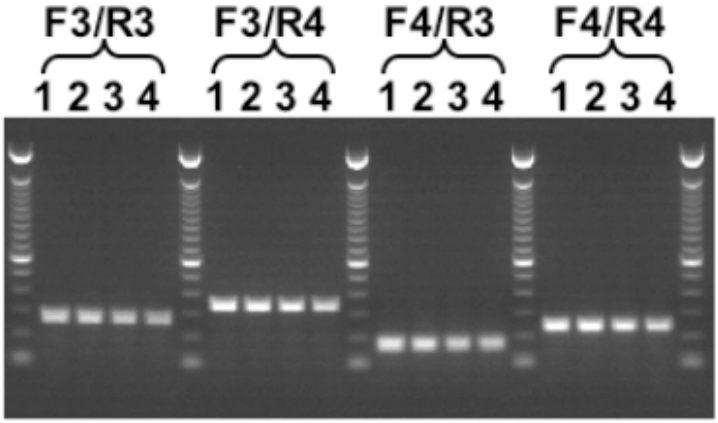
F3/R3
F3/R4
F4/R3
F4/R4
1 2 3 4
1 2 3 4
1 2 3 4
1 2 3 4

c

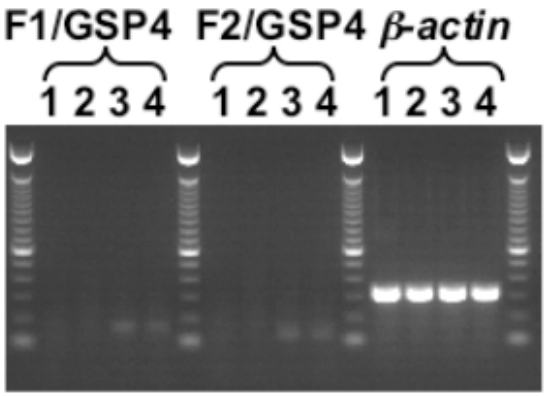
F1/GSP4
F2/GSP4
β-actin
1 2 3 4
1 2 3 4
1 2 3 4

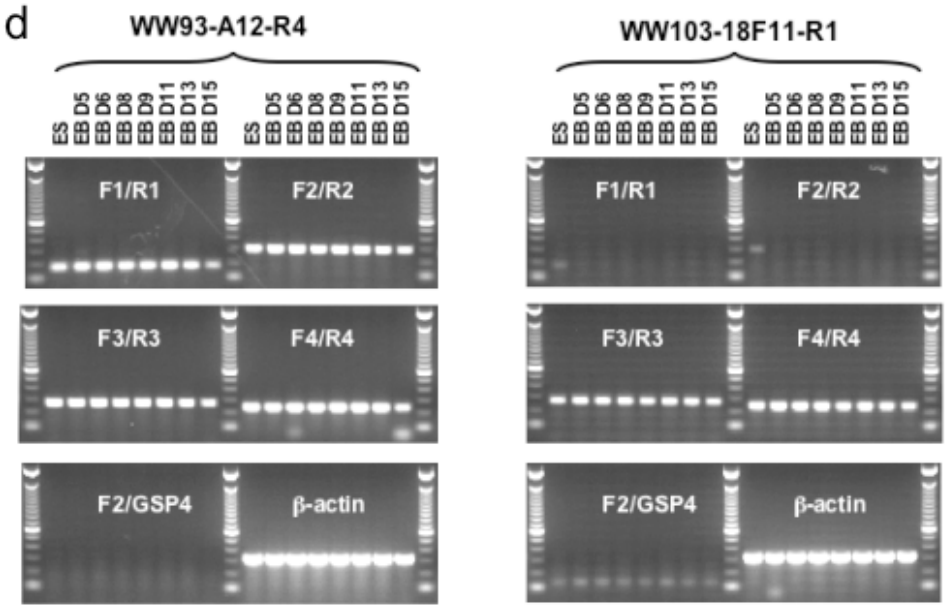

Fig. 5-12 Confirmation of WW103-18F11. a. RT-PCR to detect transcripts across the inversion breakpoint. PCR primers were designed to specifically amplify cDNA fragments from Exon 1 to Exon 2 (F1/R1 and F2/R1) and Exon 1 to Exon 3 (F1/R2 and F2/R2). RNA extracted from undifferentiated ES cells was used as template. lane 1, WW93-A12-R4; lane 2, WW93-A12-R5; lane 3, WW103-18F11-R1; lane 4, WW103-18F11-R6. RT-PCR results showed that *Acly* transcription across the inversion breakpoint was blocked. **b.** RT-PCR to detect the transcription of downstream exons. PCR primers were designed to specifically amplify cDNA fragments from Exon 24 to Exon 28 (F3/R3 and F3/R4) and Exon 25 to Exon 28 (F4/R3 and F4/R4). RT-PCR results showed that the transcription of downstream exons was not affected by the inversion. This suggests the existence of alternative transcript start points. **c.** RT-PCR to detect the Exon 1/β-geo fusion transcript. Primer pairs F1/GSP4 and F2/GSP4 were used to specifically amplify the gene trap fusion transcript. **d.** RT-PCR to detect *Acly* expression during ES cell *in vitro* differentiation. High *Acly* expression was detected in the whole process of differentiation of WW93-A12 control cell line, but not in WW103-18F11.

The modified BAC clone was linearized by I-*Sce*I and electroporated into WW103-18F11 ES cells (HAT^R, Neo^R, $Puro^R$, Bsd^S). 12 blasticidin resistant clones were picked and Southern analysis was carried out using an *Acly* gene specific probe to identify ES cell clones with a wild-type restriction fragment (Fig. 5-13c). One of the clones, WW113-2-8 has the wild-type restriction fragment and the ratio between the wild-type restriction fragment and the targeted restriction fragment is about 1:1, suggesting that this is likely to be a complemented clone which contains two wild-type copies of *Acly* gene. Another two clones, WW113-2-10 and WW113-2-11 also have the wild-type restriction fragment. But the ratio between the wild-type restriction fragment and the targeted restriction fragment is about 1:2, which suggests that both clones might contain a single copy of the BAC DNA, which can be randomly truncated and are likely to be incomplete. Western analysis was performed on whole-cell lysates extracted from undifferentiated wild-type control, *Acly*-deficient and BAC-rescued ES cells using a polyclonal rabbit anti-*Acly* antibody. *Acly* protein was not detected in the lysates from the WW103-18F11 cells. However, one of the BAC-rescued clones (WW113-8) expressed similar level of the *Acly* protein as the WW93-A12 wild-type control cells, indicating that this clone (WW113-2-8) is a rescued clone (Fig. 5-13d). The other two clones, WW113-2-10 and 2-11, which did not express *Acly* protein, are likely to only contain a truncated form of the BAC DNA and thus they were used as negative controls.

These three clones were expanded and induced to differentiate *in vitro*. After EBs were plated on the gelatinized tissue culture plates at Day 5, the EBs derived from WW113-2-8 ES cells could form cystic three-dimensional structures, while the EBs derived from WW113-2-10 and 2-11 ES cells could not (Fig. 5-13e).

a

b

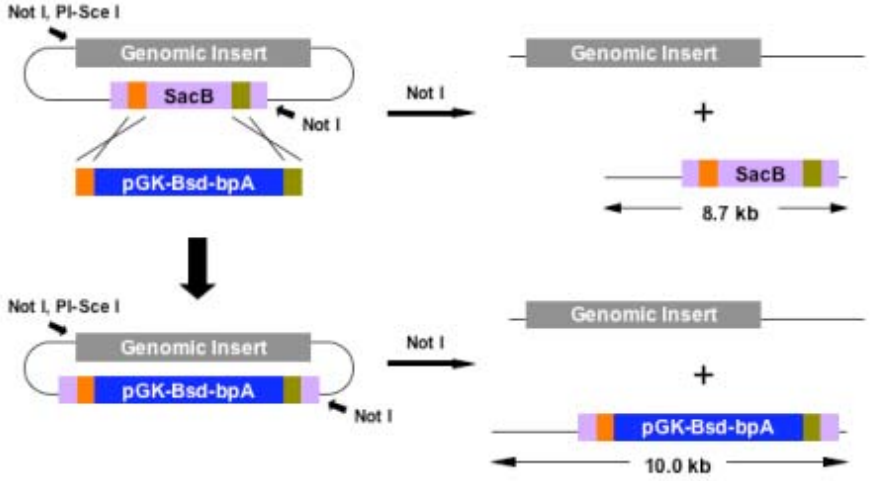
Not I, PI-Sce I
Genomic Insert
SacB
Not I
pGK-Bsd-bpA
Not I
Genomic Insert
+
SacB
8.7 kb
Not I, PI-Sce I
Genomic Insert
pGK-Bsd-bpA
Not I
Not I
Genomic Insert
+
pGK-Bsd-bpA
10.0 kb

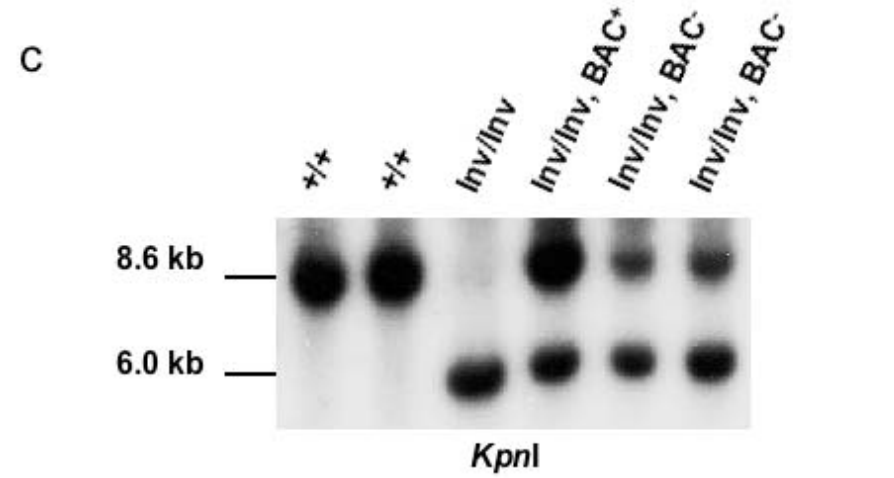
c
+/+
+/+
Inv/Inv
Inv/Inv, BAC+
Inv/Inv, BAC-
Inv/Inv, BAC-
8.6 kb
6.0 kb
KpnI

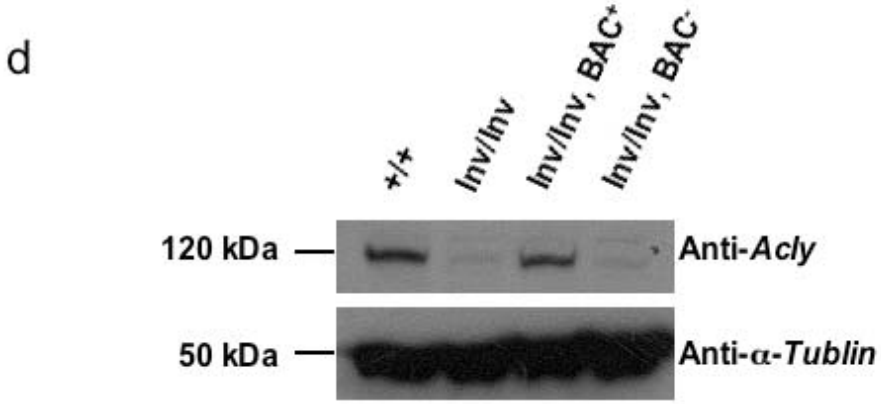
d
+/+
Inv/Inv
Inv/Inv, BAC+
Inv/Inv, BAC-
120 kDa
Anti-Acly
50 kDa
Anti-α-Tublin

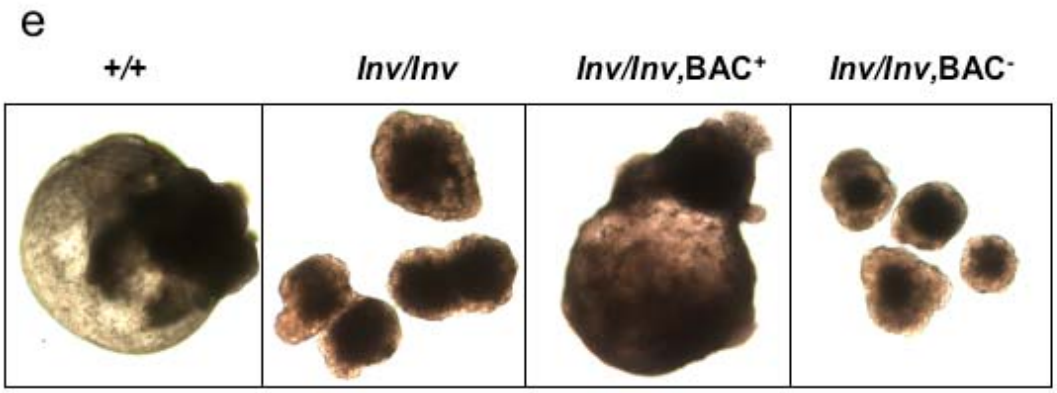
e
+/+
Inv/Inv
Inv/Inv,BAC+
Inv/Inv,BAC-

Fig. 5-13 BAC rescue. a. BAC clone BMQ-290J5. An 129 S7 BAC clone, BMQ-290J5 was picked according to the BAC end mapping information of this clone in the Ensembl database. This clone was confirmed to contain the complete *Acly* gene by PCR. BAC clone BMQ-290J5 is highlighted in blue. **b.** Insertion of a *PGK-Bsd-bpA* cassette into the BAC backbone. To facilitate the drug selection of BAC integration in ES cells, a *PGK-Bsd-bpA* cassette (pL313) was inserted into the *SacB* gene on the backbone of this BAC clone by *E. coli* recombination. **c.** Southern analysis of modified BAC clones. The correct insertion of the *Bsd* cassette into the BAC backbone was confirmed by Southern using a *SacB* specific probe. BAC DNA from the modified clones was digested with *Not*I. The *SacB* probe detected a 8.7 kb restriction restriction fragment for the unmodified BAC clone, and it detected a 10 kb fragment for the modified clones. **d.** Southern analysis of BAC inserted ES cell clones. Genomic DNA from 12 blasticidin resistant clones were digested with *Kpn*I, and Southern analysis was carried out using an *Acly* gene specific probe to identify ES cell clones with a wild type restriction fragment. WW113-2-8 (red) has the wild type restriction fragment and the ratio between the wild type restriction fragment and the targeted restriction fragment is about 1:1, suggesting that this is likely to be a complemented clone which contains two wild type copies of Acly gene. Another two clones, WW113-2-10 and WW113-2-11 (blue) have the wild type restriction fragment, but the ratio between the wild type restriction fragment and the targeted restriction fragment is about 1:2, which suggests that both clones might contain a single BAC clone which is likely to be incomplete. These two clones were used as control for the in vitro differentiation experiment.

When RT-PCR was performed on RNA extracted from WW113-2-8 embryoid bodies collected at different time points, the expression of *Oct3/4*, *Nodal* and *Nanog* were down-regulated rapidly as observed in WW93-A12 derived EBs. However, WW113-2-10 and 2-11 still expressed high level of these primitive ectoderm markers at late stages of their differentiation process (Fig. 5-14a).

The expression pattern of the early mesodermal markers (*Bmp4*, *Brachyury* and *Goosecoid*) also became normal in the EBs derived from WW113-2-8 ES cells. The expression of *Brachyury* and *Goosecoid* was down-regulated much quicker in the WW113-2-8 derived EBs than in the WW113-2-10 or 2-11 derived EBs. The expression pattern of these markers in WW113-2-8 derived EBs was similar to that observed in the control WW93-A12 derived EBs (Fig. 5-14b).

Acly gene-specific RT-PCR primer pairs have also been used to check *Acly* expression during *in vitro* differentiation of the BAC rescue cell line, WW113-2-8. In the WW113-2-8 cell line, significantly higher *Acly* expression than the other two control cell lines was observed in undifferentiated ES cells, as well as throughout the whole differentiation process. RT-PCR using the F1/GSP4 primer pair confirmed that gene-trap transcripts were still present in the rescued cell line, WW113-2-8. So the phenotype observed in the WW103-18F11 mutant cell line was caused by the loss of normal *Acly* transcription, instead of the dominant-negative effects, as the phenotypes could be reversed by re-introducing a wild-type copy of *Acly* gene (Fig. 5-14c).

All these data suggest a direct link between the reduction in *Acly* expression and the impaired *in vitro* differentiation potential observed in WW103-18F11 derived EBs.

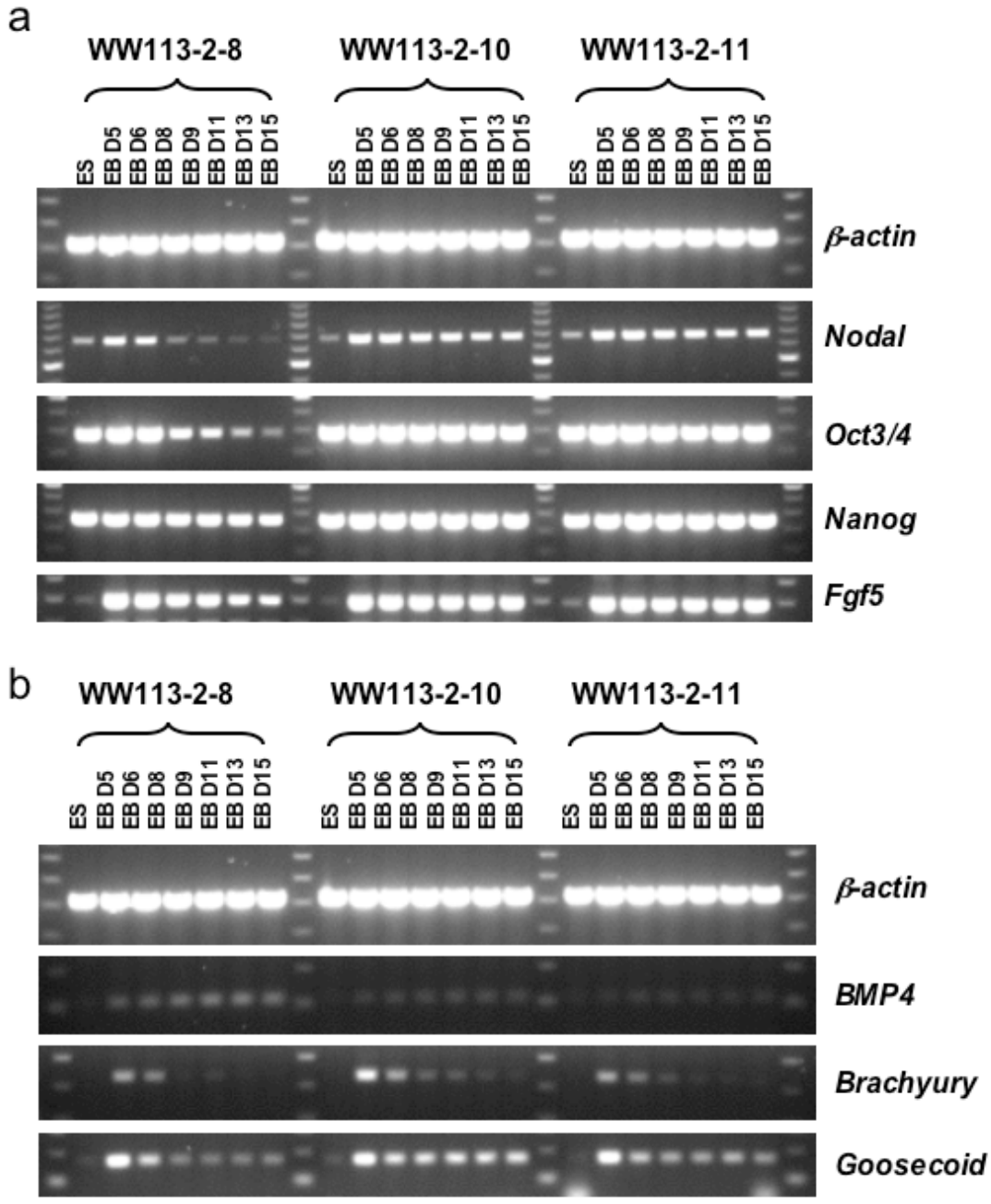
a
WW113-2-8
WW113-2-10
WW113-2-11
ES
EB D5
EB D6
EB D8
EB D9
EB D11
EB D13
EB D15
β-actin
Nodal
Oct3/4
Nanog
Fgf5
b
WW113-2-8
WW113-2-10
WW113-2-11
β-actin
BMP4
Brachyury
Goosecoid

5.3 Discussion

In this chapter, I have described how I have used ES cell *in vitro* differentiation to screen a set of homozygous mutant ES clones. A panel of 16 markers was used to carry out the primary screen. To increase the throughput of the screen, I only took samples at three time points. If a homozygous mutant ES cell clone showed abnormal expression for one or more markers, the clone was subsequently tested in the second round screen. In the second round screen, more samples were taken at different time points, and additional markers were checked by RT-PCR to confirm the authenticity of the phenotype and also try to explain the phenotype at the molecular level by the gain or loss of specific differentiation markers.

5.3.1 Throughput of the screen

In this experiment, only a limited number of homozygous mutant ES clones were used for the *in vitro* differentiation screen. Therefore, it is possible to make a large number of EBs for each cell line and take samples at multiple time points. However, if the number of cell lines for screening increases to several hundred or several thousand, it would be necessary to make tens of thousands of plates of EBs. To make hundreds of thousands of “hanging drops”, transfer them to gelatinized tissue culture plates and change media regularly will be a labour-intensive work.

The RT-PCR method is not sensitive enough for the high-throughput analysis either. Approximately 20 μg of total RNA can be extracted from a plate of 40 EBs after Day 10. But for the early EBs (Day 5 to Day 10), sometimes two or three plates of EBs need to be combined together to get enough RNA. The cDNA synthesized from 5 μg of total RNA is only enough for about 20 RT-PCR reactions. If 10 cell lines are checked at the same time, 8 time points are taken for each cell line, and 16 markers are screened, this will require 1,280 PCR reactions. Any clones that do not show an obvious abnormality in these 16 markers will be discarded which is not a thorough analysis of the differentiation potential. Also, RT-PCR is a semi-quantitative approach to

assess gene expression, which makes it difficult to detect minor changes in expression.

An alternative approach to RT-PCR is to use cDNA and oligonucleotide microarray technology, which has been well characterized and proven to be a powerful tool for large-scale screens. This technology enables one to check the expression of all the genes in the mouse genome simultaneously. The development of array technology has made it possible to use very small amounts of starting RNA template. However, the downside of this technology is that it is still very expensive and the high cost makes it impractical to screen a lot of samples. Another problem of using microarray analysis to study ES cell *in vitro* differentiation is the complexity of the input material. It would be necessary to perform many control experiments to define the normal ranges of expression levels during differentiation, before comparisons can be made with samples from the mutant lines. Fluorescent reporters and FACS can also be used to screen the mutants in a high-throughput manner. It will be further discussed in the final chapter.

Considerable data has accumulated on the expression pattern of various markers characterizing the development of the three germ layers and other differentiated cell types during the ES cell *in vitro* differentiation process. However, this data is scattered throughout the literature and is far from being systematic or comprehensive. The results in these publications were generated by various methods, including RT-PCR, Northern, *in situ* hybridization or immunohistochemistry. Different ES cell lines (feeder-free or feeder-dependent), different differentiation protocols, and different lengths of observation periods make the data generated from these different experiments difficult to compare.

So before ES cell *in vitro* differentiation is used for a large-scale *in vitro* recessive screen, a systematic, quantitative study should be performed to determine the expression pattern of important developmental and differentiation markers in the differentiation process of the wildly used ES cell lines (AB2.2, D3, R1 and E14.1, etc.). Ideally, this data needs to be compared

to the expression pattern of these markers *in vivo* to link the *in vitro* differentiation with its *in vivo* counterpart.

5.3.2 Alternative recombination

Interestingly, two clones that have shown an abnormality during *in vitro* differentiation both contain either an extra chromosome 11 (WW103-8E6) or two partial duplication chromosome 11s (WW103-13D10). As discussed in the previous chapter, some clones can undergo a G2 *trans* recombination event and the resulting duplication chromosome can become homozygous by induced mitotic recombination. These homozygous duplication clones have as many as four copies of all the genes in the chromosomal region between the gene-trap locus and the end point targeting locus (*E_2DH*, 100.7 Mb). For WW103-13D10 (*LOC217071*, 88.7Mb), the duplication region is 12 Mb. It is reasonable to expect that such a big chromosomal rearrangement will cause an abnormality in differentiation. The WW103-8E6 clone has accumulated an extra chromosome before regional trapping. The subsequent mitotic recombination has duplicated the inversion chromosome, but a wild-type chromosome with the end point targeting cassette is still present. So the phenotypes of these clones with alternative recombination events are not related to the gene-trap loci, and are caused by the duplication of a part of or the whole chromosome.

5.3.3 *Acly* deficiency and the impaired differentiation potential

Acly is an important enzyme involved in fatty acid biosynthesis. Its product, acetyl-CoA, is the key building block for *de novo* lipogenesis (Beigneux, Kosinski et al. 2004). There are at least three principal sources of acetyl-CoA: 1) amino acid degradation produces cytosolic acetyl-CoA, 2) fatty acid oxidation produces mitochondrial acetyl-CoA, 3) Glycolysis produces pyruvate, which is converted to mitochondrial acetyl-CoA by pyruvate dehydrogenase (Garrett and Grisham 1999). The acetyl-CoA from amino acid degradation is not sufficient for fatty acid biosynthesis, and the acetyl-CoA produced by fatty acid oxidation and by pyruvate dehydrogenase can not cross the mitochondrial membrane. So cytosolic acetyl-CoA is mainly generated from citrate which is transported from the mitochondria to the

cytosol. ATP-citrate lyase converts the citrate to acetyl-CoA and oxaloacetate. Acetyl-CoA provides the substrate for cytosolic fatty acid synthesis, while the oxaloacetate is converted to malate which is transported back into the mitochondria where it can be converted back into citrate (Fig. 5-15).

5.3.3.1 *Acly* deficiency in the mouse

To investigate the phenotype of *Acly* deficiency in the mouse, an *Acly* knockout has been examined. This mouse line was generated from the Bay Genomics gene-trap resource (Stryke, Kawamoto et al. 2003). In this clone, a β-galactosidase marker is expressed from *Acly* regulatory sequences. Beigneux *et al*. (2004) have found that *Acly* is required for embryonic development, because no viable homozygous embryos were identified after 8.5 dpc. The early embryonic lethality suggested that the alternative pathways to produce acetyl-CoA in the cytosol are not sufficient to support development in the absence of *Acly* during development (Beigneux, Kosinski et al. 2004).

Northern and Western analysis of *Acly* mRNA and protein showed that in all the tissues examined (liver, heart, kidney, brain, and white adipose tissue), heterozygous mice expressed half of the normal amount of *Acly* mRNA and protein. But the heterozygous mice were healthy, fertile, and normolipidemic on both normal and high fat diets. The expression of another acetyl-CoA enzyme, Acetyl-CoA synthetase 1, was not up-regulated. Thus it seems that *Acly* is synthesized in adequate quantities and half-normal amount of the enzyme is enough for providing sufficient acetyl-CoA (Beigneux, Kosinski et al. 2004).

One interesting finding is that *Acly* is expressed at high levels in the neural tube at 8.5 dpc. The fact that *Acly* is not expressed in other foetal tissues suggests that *Acly* might not function as a house-keeping gene during development. Otherwise, widespread expression of *Acly* will be detected in all the cell lineages. Instead, it might have a tissue-specific function in embryogenesis, apart from producing Acetyl-CoA for lipogenesis.

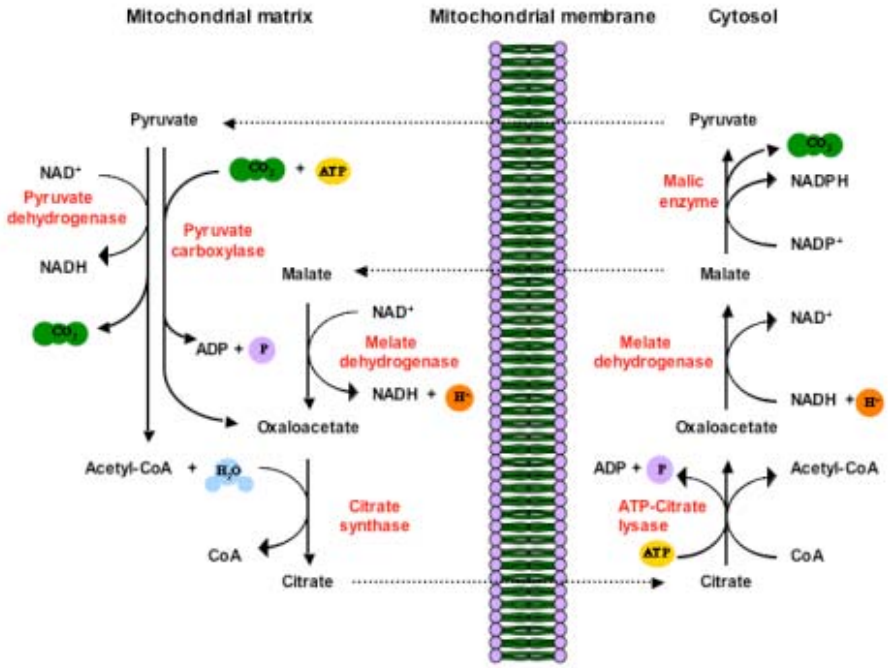

Fig. 5-15 The function of ATP-citrate lyase gene. The only known function of *Acly in vivo* is to generate acetyl-CoA by the ATP-driven conversion of citrate and CoA into oxaloacetate and acetyl-CoA. This is the first step for the *de novo* biosynthesis of sterol and fatty acid.

5.3.3.2 *Acly* and cell differentiation during sexual development

Acly has been shown to be involved in the sexual development of the fungus *Sordaria macrospora*. The fruiting body formation of filamentous ascomycetes involves the formation of the outer structures, as well as the development of mature ascospores within the fruiting body itself. Since this process requires the differentiation of several specialized tissues and some dramatic morphological and physiological changes, fruiting body maturation has been used as a model system to study multicellular development in eukaryotes (Nowrousian, Masloff et al. 1999).

Norwrousian *et al*. (1999) has used UV mutagenesis to screen for mutants with defects in fruiting body formation. One of the sterile mutants, per5, showed normal vegetative growth. But the fruiting body neck of the mutant strain was much shorter than that of the wild-type control. Most importantly, the fruiting bodies of the mutant strain only contain immature asci with no ascospores. DAPI staining showed that the immature asci still have eight nuclei within them, which suggests that there is no impairment in karyogamy or meiotic and postmeiotic divisions (Nowrousian, Masloff et al. 1999).

An indexed cosmid library was used to rescue the phenotype. A single complementing cosmid was isolated and sequence analysis has identified an ORF which has significant homology with higher eukaryotic *Acly*s. Analysis of the mutant *Acly* gene has identified a single nucleotide exchange (T to A), which altered a codon for aspartic acid into one for glutamic acid. The cloned mutant *Acly* gene can not rescue the phenotype of the mutant strain. Therefore, the mutation in *Acly* gene is responsible for the sterile phenotype (Nowrousian, Masloff et al. 1999).

As the mutant strain showed normal vegetative growth, it seems that sufficient acetyl-CoA is still produced for lipogenesis, either by residual *Acly* activity and/or expression of other acetyl-CoA-producing enzymes. But the attenuated *Acly* production can not satisfy the demand of acetyl-CoA during sexual development. So, the house-keeping functions of *Acly* can be circumvented to

a certain degree, but are essential under specific physiological conditions, such as sexual differentiation (Nowrousian, Masloff et al. 1999).

5.3.3.3 *Acly* as an *Brachyury* downstream notochord gene

Acly appears to be a downstream target of *Brachyury* in *Ciona intestinalis*. It is expressed specifically in the notochord in the embryogenesis process in *Ciona intestinalis*. The notochord has two major functions during chordate embryogenesis, providing inductive signals for the patterning of the neural tube and paraxial mesoderm and supporting the larval tail. The *Brachyury* gene encodes a transcription factor which contains a T DNA-binding domain. In vertebrates, *Brachyury* is first expressed in the presumptive mesoderm, and its expression is gradually restricted to the developing notochord and tailbud. *Brachyury* is believed to be one of the determinants for posterior mesoderm formation and notochord differentiation (Hotta, Takahashi et al. 2000).

By expressing the *Ciona intestinalis Brachyury* gene, *Ci-Bra*, in endoderm cells, Hotta *et al*. (1999) have isolated cDNA clones for 501 independent genes that were activated by *Ci-Bra* mis- and/or overexpression. By *in situ* hybridization, nearly 40 genes were found to be specifically or predominantly expressed in notochord, and therefore suggested to be *Brachyury*-downstream genes involved in notochord formation and function (Hotta, Takahashi et al. 1999). One of these genes, *Ci-Acl*, was found to share a high degree of homology with human ATP-citrate lyase (*ACLY*). The expression of this gene was first detected at the neural plate stage by *in situ* hybridization and its expression is restricted to notochord cells (Hotta, Takahashi et al. 2000). The fact that *Ci-Acl* only begins to express at the neural plate stage suggests that this gene might not be the immediate or direct target of *Ci-Bra*. Instead, it might be regulated by transcription factors, which in turn are regulated by *Ci-Bra* (Hotta, Takahashi et al. 2000).

It is interesting to notice that during embryogenesis of *Ciona intestinalis*, the expression of *Acly* is also highly restricted, similar to its expression pattern in murine embryogenesis. Considering the function of notochord in the

patterning of neural tube and paraxial mesoderm, it is likely that in both organisms, *Acly* plays some roles in neural tube and mesoderm differentiation.

5.3.3.4 Radicicol binds and inhibits mammalian *Acly*

Radicicol was first isolated from *Monosporium bonorden* as an antifungal antibiotic. But recently, this chemical was found to be able to reverse the transformed phenotype in *src*, *ras*, *mos*, *raf*, *fos*, and SV40-transformed cell lines. It can also cause cell cycle arrest and inhibit *in vivo* angiogenesis. So radicicol and its derivative are considered to be potential anti-cancer drugs (Ki, Ishigami et al. 2000).

To identify the *in vivo* target molecule of radicicol, Ki *et al*. (2000) used an affinity matrix to isolate radicicol-binding protein. Radicicol was biotinylated at various positions, and these variant compounds were then tested for their activity of morphological reversion of *src*-transformed phenotype. Two of the compounds, BR-1 and BR-6 were found to retain the activity. BR-6 was found to bind a 90-kDa protein, which was identified to be *Hsp90* by immunoblotting. BR-1 was shown to bind another 120-kDa protein, whose internal amino acid sequence was identical to human and rat ATP-citrate lyase. The identity of this 120-kDa protein was then confirmed by immunoblotting. Kinetic analysis showed that the activity of rat ATP-citrate lyase was inhibited by radicicol and BR-1, but not by BR-6. Radicicol was also found to be a non-competitive inhibitor of ATP-citrate lyase (Ki, Ishigami et al. 2000).

The fact that two radicicol derivatives, BR-1 and BR-6, bind two different proteins *in vivo* suggests that radicicol can bind different targets through different portions of its molecular structure. But the K_i value for ATP-citrate lyase was higher than the effective concentration of radicicol to reverse the transformed phenotype in *src*-tranformed cells, which suggests that this enzyme might not be directly involved in this process (Ki, Ishigami et al. 2000). Ki *et al*. (2000) hypothesized that BR-1 might be not stable and may be cleaved *in vivo* to generate free radicicol (Ki, Ishigami et al. 2000). But it could also be possible that radicicol is modified or cleaved *in vivo* to generate more

potent molecules to inhibit the enzyme activity of ATP-citrate lyase. Thus the phenotypes of radicicol, especially the ability to reverse the transformed phenotype in the cancer cell lines, might be partially associated with its binding and subsequent inhibition of *Acly* protein.

5.3.3.5 *Acly* is an important component of cell growth and transformation

Stable knockdown of *Acly* leads to impaired glucose-dependent lipid synthesis and also impaired *Akt*-mediated tumorigenesis (Bauer, Hatzivassiliou et al. 2005). Mammalian cells can not autonomously utilize the environmental nutrients to sustain their growth. Instead, constant extracellular signalling is needed to regulate the cellular metabolism of nutrients. However, cancer cells gain the autonomous ability to utilize nutrients by constitutively activating the normal signalling pathway without extracellular signals.

PI3K/*Akt* signalling pathway is critical for the cytokine-stimulated glucose metabolism, and its constitutive activation is commonly observed in cancer cells. In mammalian cells, glucose can either be oxidized to generate bioenergy, or be converted into other macromolecules to support biosynthesis. PI3K/*Akt* pathway can regulate the conversion of glucose to lipid and thus is essential for channeling the glucose into biosynthesis pathways. *Acly* is the main enzyme for producing cytosolic Acetyl-CoA for lipogenesis, and it is phosphorylated by *Akt in vivo* (Berwick, Hers et al. 2002). So it is possible that *Akt*-dependent cell transformation depends on *Acly* for *de novo* lipogenesis.

Bauer et al. (2005) used a shRNA construct to stably knock down the expression of *Acly* in a *Akt*-transformed cell line, FL5.12. *Akt*-expressing cells with or without *Acly* knockdown were injected into nude mice intravenously, and the mice were monitored for Akt-dependent leukemogenesis. Mice administrated *Acly* knockdown cells exhibited a significant delay or even a complete resistance to leukemogenesis.

5.3.3.6 A possible explanation of the phenotype of *Acly* deficient ES cells

Our *in vitro* differentiation results and works published before (Hotta, Takahashi et al. 1999; Nowrousian, Masloff et al. 1999; Hotta, Takahashi et al. 2000; Ki, Ishigami et al. 2000; Bauer, Hatzivassiliou et al. 2005) all suggested a pivotal function of *Acly* in cell differentiation and transformation. The only known function of *Acly in vivo* is to generate acetyl-CoA by the ATP-driven conversion of citrate and CoA into oxaloacetate and acetyl-CoA. This serves as the first step for the *de novo* biosynthesis of sterol and fatty acid. So the housekeeping function of the gene should be important for cell survival. But our observation and other published works (Nowrousian, Masloff et al. 1999; Beigneux, Kosinski et al. 2004) suggested that the house-keeping function of this gene can be circumvented to some degree either by the residual *Acly* activity or other alternative acetyl-CoA producing pathways.

In this study, there is no apparent difference in the growth rate, colony formation ability or ES cell/colony morphology in *Acly*-deficient ES cells compared to the wild-type control (data not shown). Microarray analysis using RNA extracted from undifferentiated WW103-18F11 and WW93-A12 ES cells showed that the expression levels of most mouse genes are similar (this work is still ongoing), which suggests that *Acly* deficiency does not cause observable phenotype in ES cells and the acetyl-CoA production in *Acly*-deficient ES cells seems to be sufficient to sustain the normal growth and division of ES cells.

However, when the *Acly*-deficient ES cells were differentiated *in vitro*, they could not form the typical three-dimensional cystic structures. In addition, the expression of some germ layer and cell type specific markers had changed. The RT-PCR results suggested that most cells in the cell aggregates were still undifferentiated ES cells. It is possible that the transition from the normal ES cell growth/division to the drastic re-programming and cell fate determination in the differentiation process demands higher than normal amounts of acetyl-CoA. A similar situation might accompany the transition from vegetative to sexual development in *S. macrospora* (Nowrousian, Masloff et al. 1999). It is

possible that this energetic demand can not be fulfilled by the alternative metabolic pathways, which might be partly due to different metabolic costs of lipogenesis.

Another possible explanation is that in order for some ES cells in an EB to be differentiated into a certain cell type, these cells must gain “competence” before the differentiation process is induced. The differentiation competence might involve as one component a threshold in acetyl-CoA concentration, which might be much higher than the level that is necessary for the ES cell growth and division.

The exact mechanism by which the acetyl-CoA production can influence the potential of ES cells to differentiate *in vitro* is unknown. Acetyl-CoA can be used to produce fatty acids, sterols and other important molecules which need the acetyl base, such as acetylcholine (Beigneux, Kosinski et al. 2004). Therefore, ATP-citrate lyase may either control the overall cytosolic acetyl-CoA concentration to indirectly regulate the pathways that need acetyl-CoA, or it could directly interact with various acetyltransferases or lipid/sterol synthetases to form an enzyme complex to provide acetyl-CoA. Nevertheless, *Acly* seems to play an important role in development and differentiation of certain cell types.

The difficulty to determine the primary locus of action of *Acly* make it hard to link this gene directly with any known genetic pathways controlling ES cell differentiation. It is not unexpected for mutants identified by such a genetic screen. However, if more homozygous ES cell mutants are generated in the future and screened using the same strategy, it will be possible to group the mutants by their apparent defects and study the relationships between the mutants with similar phenotypes. The importance of a genetic screen is that it can not only fill in the gaps in a known pathway, but also identify new pathways that are not necessarily overlapping with the known ones.

5.3.3.7 Future experiments to identify the function of *Acly* in ES cell *in vitro* differentiation

The RT-PCR results detected transcription of *Acly* downstream exons in the mutant line. Since *Acly* is a large gene (51.54 kb), it is possible that there are other alternative transcription start points. The proviral insertion and the subsequent inversion might not completely block all the *Acly* transcripts, so the mutation generated in the homozygous mutant cell line might not a null allele. To resolve this, a homozygous *Acly* gene targeted ES cell line can be constructed and these ES cells can be differentiated to confirm the function of the gene in ES cell *in vitro* differentiation.

To investigate the *in vivo* differentiation potential of the WW103-18F11 ES cell line, 1X 10^7 undifferentiated WW103-18F11 and control WW93A12 ES cells were injected subcutaneously into both flanks of 8-week old F1 hybrid mice (129 S7/SvEv$^{\text{Brd-}Hprtb\text{-}m2}$ X C57$^{\text{TyrBrdC1}}$ female). The animals were examined periodically over 4 weeks for the appearance and growth of tumours. 4 weeks after injection of ES cells, the mice were sacrificed, and the size of each tumor was measured after dissection. Tumor samples were cut into two halves, one half was fixed in 10% formalin for histopathological analysis, and the other half was dissected into several pieces (depending on its size) and snap-frozen in liquid nitrogen for subsequent RNA and DNA extraction.

For the WW93-A12 ES cell line, tumours were found at every ES cell injection site (8/8). Though the size of the tumours varied, all the tumours collected were dark red and highly vascular. When the tumours were bisected, a fluid filled central cavity was always found in the centre of the tumour. In contrast, for the WW103-18F11 ES cell line, only 3 tumours were found 4 weeks after the injection (3/8). All three tumours were very small and pale. No blood vessels were found on their surface. When the tumours were bisected, no fluid filled cavities were present.

Histopathology results of three tumours generated from WW103-18F11 cells and eight cases of WW93-A12 teratocarcinomas have confirmed that the differentiation potential of WW103-18F11 clones were greatly impaired

(pathology analysis was performed by Dr. Madhuri Warren). The WW103-18F11 tumours are circumscribed mixed ganglier/neuroepithelial tumours plus embryonal carcinoma composed predominantly of nests of mature glial cells with scarce neuroepithelial differentiation in the form of Homer-Wright rosettes. Nests of undifferentiated embryonal carcinoma (ES cells) are also seen. There was no evidence of differentiation into other germ cell lineages.

All the WW93-A12 tumour are circumscribed immature teratocarcinomas composed predominantly of immature glial tissue and tissues from all three germ layers: simple cuboidal epithelium, columnar epithelium, ciliated respiratory type epithelium, mucin secreting gastrointestinal epithelium; cartilage, osteoid, immature neuroepithelium, smooth muscle; and stratified squamous epithelium. In some samples, nests of immature embryonal carcinoma (undifferentiated ES cells) and isolated syncytiotrophoblast cells were also found.

We have also injected the BAC rescued ES cells into the F1 hybrid mice and are now waiting for the pathology results of the teratocarcinomas generated by subcutaneous injection. For the rescued cell line, tumours were found at every ES cell injection site (8/8). All of the tumours were dark red and highly vascular. Some of these tumours have a fluid filled central cavity in the centre of the tumour.

From the initial result, we can conclude that the differentiation potential of the *Acly*-deficient ES cells is also impaired *in vivo*. But complete pathology results of the tumours derived from the rescued cells are needed to confirm that the *in vivo* differentiation potential is fully recovered in these cells.

Because the phenotype of the *Acly*-deficient ES cells may depend on some mutations or silencing in a second gene, inactivation of *Acly* in an independent ES cell clone is necessary to prove that the *Acly* gene is solely responsible for the differentiation defect we observed in WW103-18F11 deficient cell line. Although BAC rescue experiment can make a causal link between the mutation in *Acly* gene and the defective phenotypes, it is

possible that other genes or transcriptional elements also play some roles in the differentiation defects. If over-expression of *Acly* cDNA can also rescue the defective phenotypes, it will effectively exclude the involvement of other genes or transcriptional elements.

5.3.4 Summary

In this chapter, I have described the strategy used to screen for an *in vitro* differentiation phenotype in homozygous mutant ES cell lines. Restricted by the detection method, I checked the expression of a limited number of markers in the differentiation process. In spite of this limitation, I successfully identified several clones with a reproducible *in vitro* phenotype. By Southern analysis and sib-selection using different drugs, I found some of these clones are the products of alternative recombination events. But two of the clones, WW103-14F11 and WW103-18F11, are products of regional trapping and subsequent inversion. Detailed expression analysis and functional studies have been carried out on WW103-18F11. The impaired *in vitro* differentiation potential observed in this clones was caused by the disruption of the ATP-Citrate lyase (*Acly*) gene. Therefore, this strategy has proved to be able to identify *in vitro* differentiation mutants and facilitate regional screens for genes involved in the early embryogenesis in the mouse genome.